Preventive-corrective contingency control of distribution power grids using convolutional neural networks

W.J. Treurniet

Master of Science Thesis

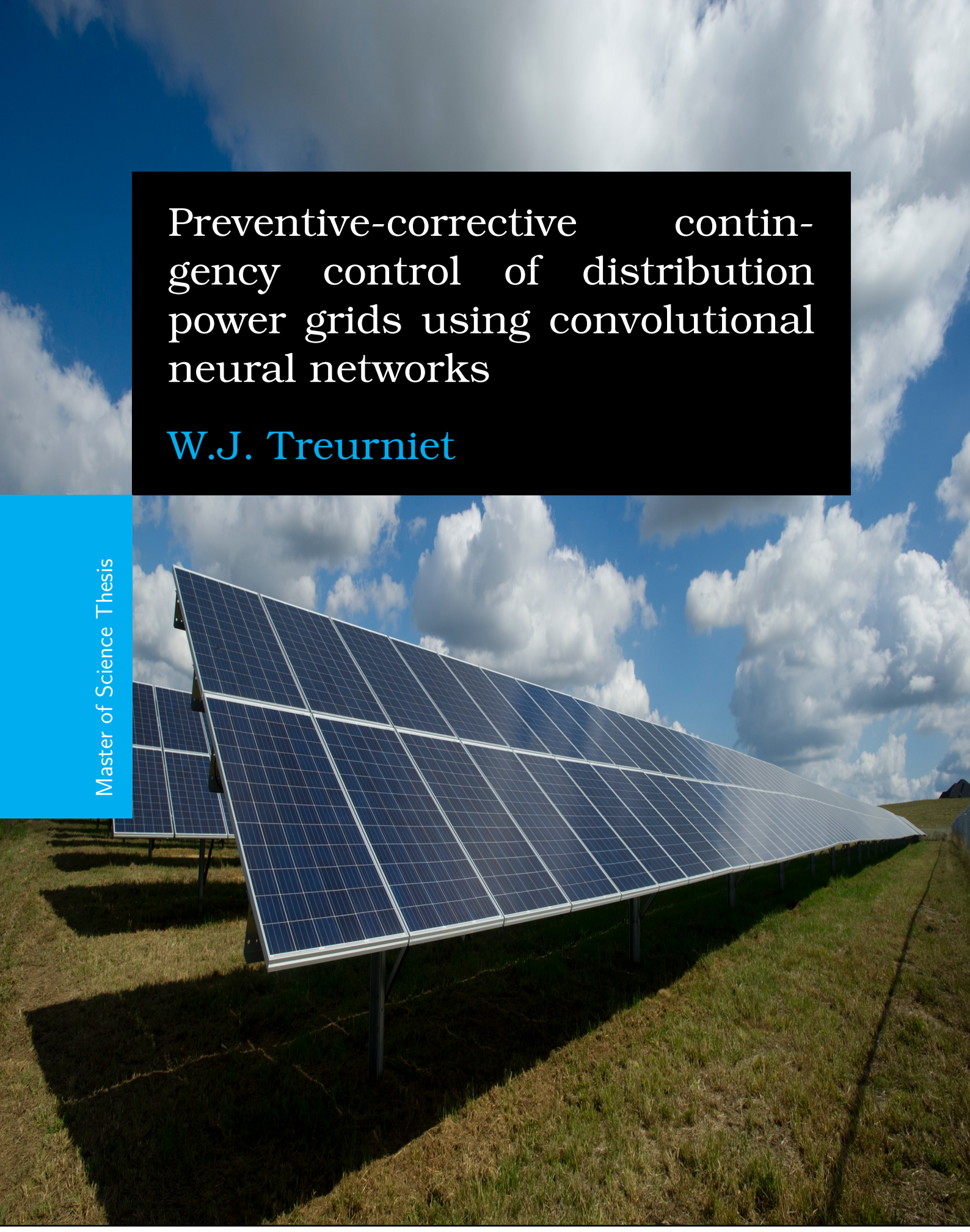

TU Delft Delft University of Technology

Delft Center for Systems and Control

Preventive-corrective contingency control of distribution power grids using convolutional neural networks

Master of Science Thesis

For the degree of Master of Science in Systems and Control at Delft University of Technology

W.J. Treurniet

January 10, 2022

Faculty of Mechanical, Maritime and Materials Engineering (3mE) · Delft University of Technology

The work in this thesis was supported by Stedin Netbeheer B.V. Their cooperation is hereby gratefully acknowledged.

Abstract

To achieve the goals on greenhouse gas emissions, the energy supply and demand is in transition. Distribution power grids therefore are increasingly reaching their capacity limits due to electrification and the vast increase of distributed energy resources (DER) connection requests with large peak power output. Increasing physical grid capacity is a costly operation and take lots of time to realise. Grid operators are therefore allowed to connect additional energy resources to the power grid at the cost of $N-1$ reserve capacity. Having $N-1$ reserve capacity means that any grid component can go out of service, without causing overloading of another grid component. When this security principle is abandoned, coupled preventive and corrective control measures might be necessary to preserve security of energy supply. In this thesis, commissioned by the Dutch distribution grid operator Stedin Netbeheer, a preventive-corrective contingency control method based on differential evolution (DE) is designed to increase the maximum admissible DER generation on a distribution grid. For the contingency analysis process in this contingency control method, the full AC power flow method is compared to the method based on line outage distribution factors. The resulting DE-based preventive-corrective control method using the full AC power flow contingency analysis method allows for significant extra DER generation capacity to be connected to the study case distribution power grid, without requiring expensive grid expansions. The case study of this thesis work is the Stedin Middelharnis distribution power grid. Due to the computational complexity of the preventive-corrective contingency control method and the sparse connectivity of power system data, convolutional neural networks are deployed to reduce the computational time. In the first approach, the convolutional neural network is used to perform contingency analysis. Due to this neural network approach, the time to compute the preventive-corrective control actions is reduced by 40%. However, the accuracy of the control is significantly reduced due to the inaccuracy of the used contingency analysis method. In the second approach, a neural network is trained to determine the coupled preventive control actions. The performance of a neural network with and without convolutional neural networks is compared in this approach. Results show that the convolutional neural network outperforms the neural network without convolutional layers. This second convolutional neural network approach is satisfactory accurate and the computational efficiency of this control method is greatly increased compared to the control method based on DE, making realtime preventive-corrective control possible.

Table of Contents

Preface

This thesis work concludes my time as a student at the Delft University of Technology. It has certainly been a turbulent period, filled with moments of joy, but also shadowed by moments of pain and sorrow. I'm delighted to be able to finish my master's programme by means of this thesis work. I enjoyed working on this relevant topic related to the Dutch energy transition and hope I can continue to work on similar topics in the future.

Although this last year felt like a lone journey sometimes, I thoroughly realise that finishing this thesis would not have been possible without some important people around me.

First of all, I would like to thank professor Bart De Schutter for his guidance throughout this process. You managed to steer me into valuable directions with just a few concise remarks in the meetings that we had. Next to this, I am very grateful for my daily supervisors, Edward Coster and Bart Kers from Stedin. Your insights on electrical engineering and grid operation practices were essential, but above all, I've always felt really comfortable when meeting you and enjoyed the spare moments we met at the Stedin office. Also thanks to Hossein Khalilnezhad for his supervision in the early stages of my thesis work.

There are definitely more people in my life without whom I would not have been able to succeed. Most notably, I'd like to thank Annemé for her unceasing support throughout all the good and bad times. I know I've not been easy to live with, especially in the final stages. I admire your persistent patience and unconditional love. Besides, I'm thankful for my family and friends, who have been interested in my work throughout the process but have also offered me the distraction and social contact I desperately needed from time to time.

Wiljo Treurniet

's Gravenhage,

January 2022

Chapter 1

Introduction and background

Earth's climate is changing rapidly in every region and across the whole climate system and the role of human influence on this is undisputed, according to the latest International Panel on Climate Change (IPCC) report [21]. In an effort to combat the global challenges associated with climate change, world leaders from all across the world signed the Paris agreement in 2015 [45]. The governments agreed to substantially reduce global greenhouse gas emissions to limit the global temperature increase in this century. In the Glasgow Climate pact, signed in 2021, the countries agreed to increase their effort and to phase down the use of coal in energy production [46]. The Dutch government set a goal to reduce the Dutch greenhouse gas emissions by 49% by 2030, compared to the 1990 levels, and a 95% reduction by 2050 [18]. The above developments cause this world and The Netherlands in particular to be in the middle of an energy transition from fossil-based systems of energy production and consumption to renewable energy sources, like wind and solar energy. This ambitious and progressive energy transition poses power grid capacity challenges, as is described in Section 1-1. From these challenges, a problem statement is abstracted in Section 1-2, which is faced in this research. To face this problem, specific research objectives and research questions are presented in Section 1-3 and finally, the outline of the rest of this thesis is given in Section 1-4.

1-1 Grid capacity challenges in facilitation of the energy transition

To achieve the goals on greenhouse gas emission reductions, the energy supply and demand is in transition. Different sectors, such as mobility and built environment, are electrifying and power grids are increasingly penetrated by distributed energy resources (DER), such as photo-voltaic systems or wind turbines. Conventionally, the distribution power grid is designed in a uni-directional fashion. Power was generated by large-scale centralized generators, powered by fossil fuels such as natural gas and coal. This power was transported through the transmission network, into the distribution network. In the distribution network, the power was distributed mostly radial and uni-directional. Demand and supply was easy to balance by means of the day-ahead and intra-day energy market. This distribution network was designed to be able to deal with peak moments in terms of energy demand, with limited risk of congestion. Required physical grid investments were easy to predict years ahead and relatively low-cost. In grid codes, the $N-1$ reliability principle was and still is widely used to ensure security of supply in case of contingency or maintenance. This principle means that secure grid operation is maintained when failure of any component in the grid occurs, which is generally ensured by oversizing the grid. In The Netherlands, this principle is mandatory for high voltage (>110kV) grids. For lower voltage distribution grids, the principle is widely used as well. Since DER typically have a high simultaneity, leading to a generator power input at moments of heavy wind and solar radiation, extensive grid enhancements are required. Furthermore, due to the increased penetration of DER, the distribution grid now acts as a bi-directional network more than ever before, where moments of net supply and demand vary regularly. The power flow on the power grid is therefore more complex to determine and predict and accurate analysis of grid performance requires an extensive monitoring and communication infrastructure, which is currently not present. Overall, these developments require extensive grid expansions of the electricity grid. However, these improvements are costly and take time.

It is a challenge to improve the grid in time and at reasonable cost for society. In The Netherlands, grid operators have announced several regions where there is no room for new DER connections, so new photo-voltaic energy connections are declined or postponed [29]. The number of such regions is increasing, and the grid operator Stedin Netbeheer just announced another locked region [40]. In the Middelharnis region on the island of Goeree-Overflakkee, no grid capacity to connect DER is available. In Fig. 1-1 and Fig. 1-2, the current status of congestion is visualised for respectively the area of The Netherlands and Stedin Netbeheer.

In an response to the current and upcoming congestion on the distribution grids, the Dutch national government now allows Dutch grid operators to connect more DER using the $N-1$ reserve capacity [15]. However, when the $N-1$ reserve capacity is used for extra DER connections, parts of the power grid could possibly get congested in case of a grid component contingency. This could cause overheating of grid components, security system triggers leading to local blackouts or voltage instability.

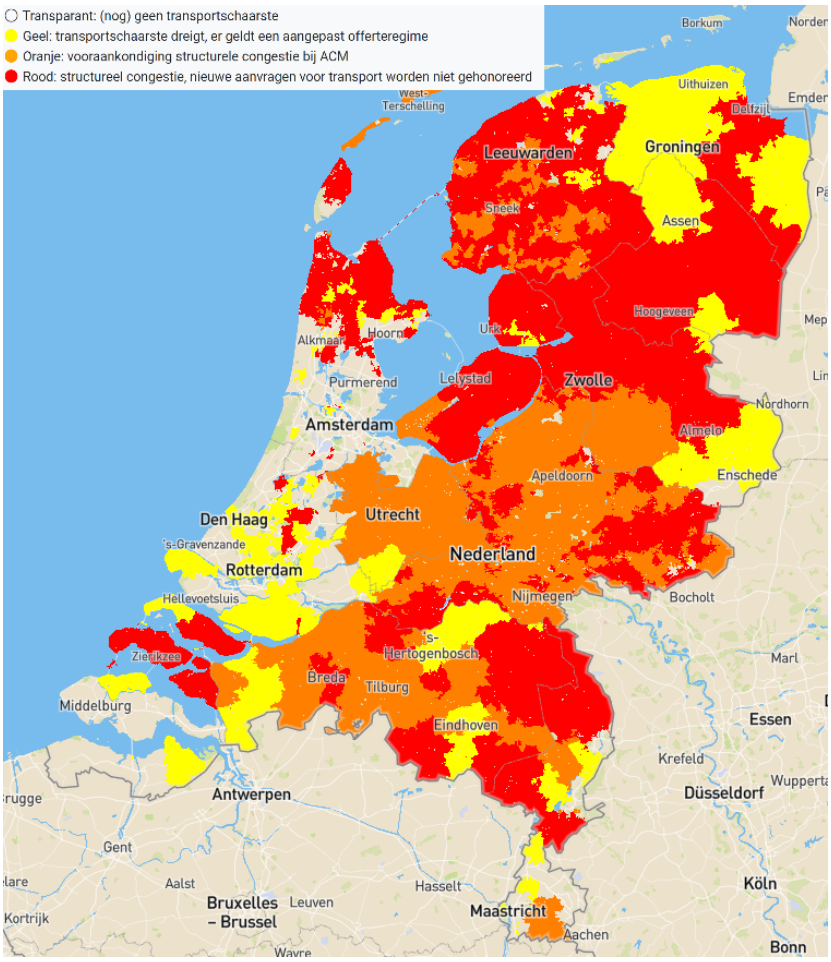

Figure 1-1: Grid congestion situation for The Netherlands, from [30].

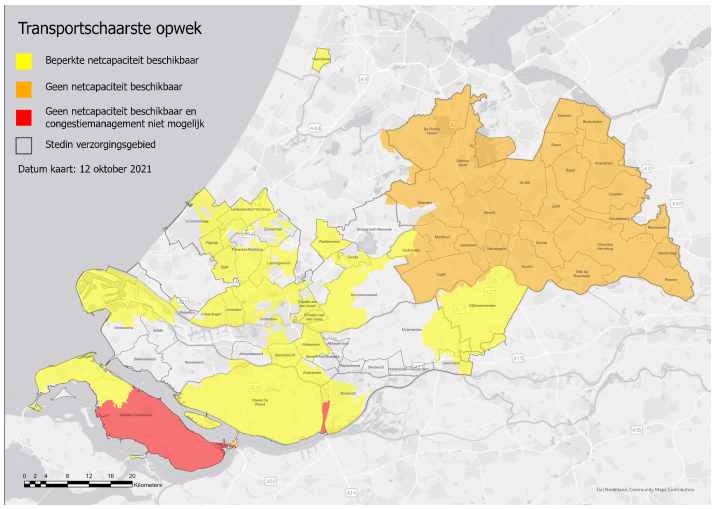

Figure 1-2: Grid congestion situation for Stedin's area, from [39].

1-2 Problem statement

From the above-mentioned grid capacity challenges, a clear problem arises:

> Distribution power grids are increasingly reaching their capacity limits due to electrification and the vast increase of DER connection requests with large peak power output. Increasing physical grid capacity is a costly operation and take a considerable amount of time to realise. Grid operators are therefore allowed to connect additional energy resources to the power grid at the cost of $N-1$ reserve capacity. However, this might cause risks in the security of supply in case of contingencies.

1-3 Research objective and research questions

The problems of overheating of grid components, voltage instability and security system triggers in case of contingency could be mitigated by means of contingency control. In contingency control, certain control measures are taken to prevent grid limits to be violated. The most common control measures are active or reactive power curtailment of generators [2, 8, 12, 20, 57, 59], load shedding [37, 57] and network topology switching [7]. These control actions can be applied after a contingency occurred, i.e. corrective control, or before a contingency occurred to prevent grid limit violations directly after the contingency, i.e. preventive control. Naturally, a combination of preventive and corrective control actions can also be applied. In literature, this combination of preventive and corrective control actions is called preventive-corrective control and is researched by multiple authors [8, 54, 55, 57]. However, the computational complexity of these control methods is large, due to the coupling between the preventive and corrective control actions. However, several efforts in literature have shown that machine learning can reduce the required realtime computational effort in power system control [5, 11, 22, 58].

> The research objective of this thesis is therefore to develop a preventive-corrective contingency control method to increase the maximum admissible DER generation on a distribution grid and to improve the computational efficiency using machine learning techniques.

To reach this research objective, the following questions will be answered:

- Within which time frame can preventive-corrective contingency control be performed?
- To what extent is the maximum admissible DER generation on a grid influenced by using preventive-corrective contingency control?
- What is the influence of using machine learning on the accuracy and computational efficiency of preventive-corrective contingency control?

1-4 Outline

In this study, a case study will be performed on the selected control methods to analyse the efficiency and accuracy of these methods and therefore to be able to answer the research questions. This case study will be performed on relevant distribution grids. The description of this case study is given in Chapter 2. The preventive-corrective control method based on iterations between the preventive and corrective control actions is described in Chapter 3. This method is tested on the case study and the results are presented and discussed in the same chapter. Then, the influence of using a machine learning technique is discussed in Chapter 4. The same case study is used to analyse the performance of this technique. Concluding remarks on both the classical preventive-corrective method and the machine learning-based methods are made in Chapter 5, where recommendations for further research are also presented.

Chapter 2

Case study description

The preventive-corrective contingency control methods developed in this study will be tested on a case study. The goal is to develop a case study which represents the situation of distribution grids in The Netherlands. Therefore, a Stedin distribution power grid is selected as main test grid for this case study. This power grids is discussed in Section 2-1. The aim for this Stedin power grid is to perform preventive-corrective contingency control within one minute. This way, the unnecessary curtailment of distributed energy resources (DER) generators and the risk of post-contingent limit violations is small. Within this minute, the power grid can be considered stationary, since the demand and supply of the power grid do generally not change drastically within a one minute time frame. To increase the insights of the influence of different design choices, several benchmark power grids are also used in this study. These power grids are also discussed.

In this chapter, the case study on which the contingency control methods will be applied is presented. To this extent, the relevant power grids are listed in Section 2-1 and the load and generation data of these power grids is presented in Section 2-2.

2-1 Power grids

The following power grids will be used to study the control methods as described in the previous chapter. The Stedin Middelharnis power grid as described in Section 2-1-1 forms the basis for this case study. In addition to this power grid, academic benchmark grids will be used for particular parts of the case study. These grids are presented in Section 2-1-2.

2-1-1 Stedin Middelharnis power grid

The Middelharnis distribution power grid is selected to provide a realistic case study, which allows for a more reliable analysis of the performance of the algorithms on Stedin's power systems. In collaboration with Stedin's representatives, a model of the Middelharnis high

voltage distribution grid is selected as test system for this research. This 50kV and 13kV distribution grid is shown in Fig. 2-1. This section of Stedin's distribution grid faces congestion issues, due to the DER generation input. Permits for new DER projects are currently not issued, to prevent increased congestion. To analyse the potential benefits of smart preventive-corrective contingency control, four extra non-firm DER connections are connected to the Middelharnis power grid. These four connections will be the controllable generators. They are placed at the locations marked in Fig. 2-1. The installed capacity for each connection is 60MWp. Connections 2 and 3 are placed in a east-west configuration. More information on this configuration can be found in [25]. Connections 1 and 4 are faced to the south. For this case study, it is assumed that the controllable generators can only be curtailed for 20% of their maximum power output per minute. This coincides with the regulations as found in the Dutch grid code [3]. Furthermore, it is assumed that any loading or voltage violations should be mitigated within 30 seconds after a contingency occurred. This results in a limited time to perform corrective control and hence couples the preventive control actions to the corrective control actions, which requires preventive-corrective control.

The number of contingencies considered for this power grid is 12. Only non-islanding contingencies are considered, since otherwise the security of supply is lost regardless of any control actions.

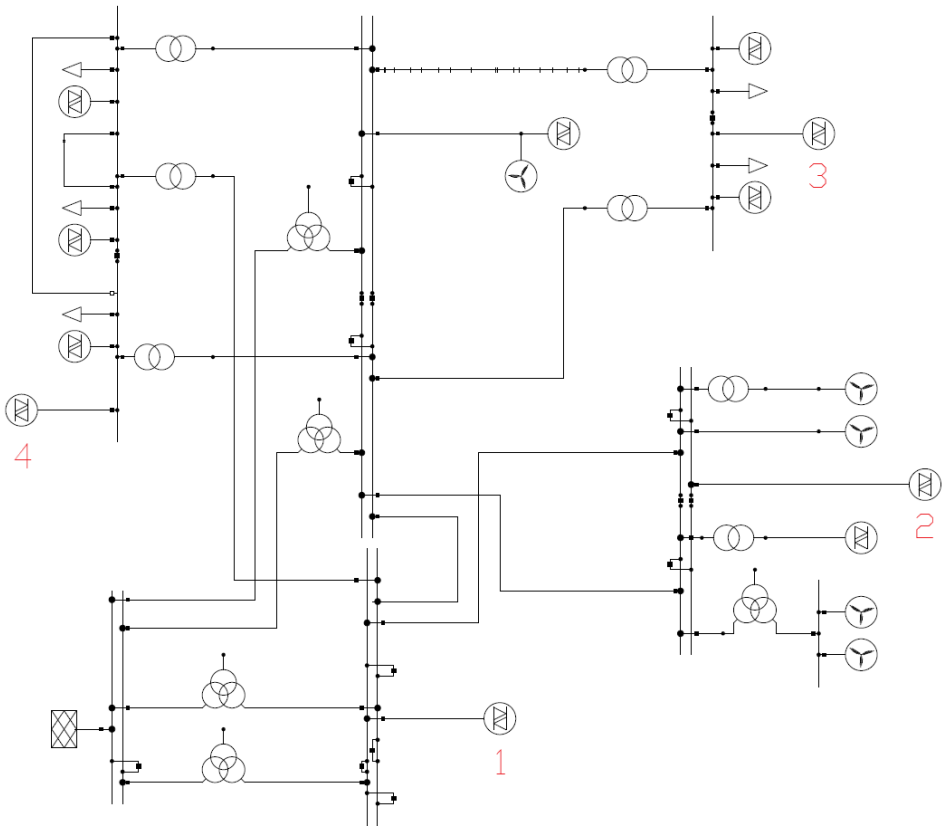

Figure 2-1: Stedin Middelharnis power grid with additional DER marked by numbers.

2-1-2 Academic benchmark grids

In addition to the Stedin Middelharnis power grid, academic benchmark power grids will be used in this research to validate some of the used methods. This is done to analyse the influence of the size of the networks to the performance of the different methods. The three different used academic benchmark power grids are discussed below.

IEEE 9-bus power grid

The IEEE 9-bus power grid is a small sized transmission power grid, first used and published by [32]. The grid is shown in Fig. 2-2 and consists of nine buses, three loads and three synchronous generators. This benchmark grid can provide useful information on the performance of methods on a small scale. Contingency of all lines in this system is considered, so the number of considered contingencies is 6.

CIGRÉ MV power grid

The CIGRÉ MV test system as shown in Fig. 2-3 is suitable for this research. It is a 20kV AC power system, most commonly used for control purposes in literature. This network is connected to the transmission grid via a slack bus. The system is weakly-meshed and includes multiple switches. These switches could be controlled or considered closed or open at all times. If the switches are considered open at all times, the system reduces to a radial system. To ensure supply of power for all contingencies, the switches will be closed for this research. This test system is presented in detail in [9]. It is mentioned that network voltage level, line lengths, types and parameters and load values can be adjusted as necessary, though voltage level changes requires the conductors, transformers, etc. to be adjusted accordingly. In [34], this CIGRÉ MV network is used to design a benchmark distribution network for investigation of integration of DER. Part of the scope of this benchmark is to allow for studies on energy management systems for DER in the MV distribution network. In the article, a wind turbine, photovoltaic systems, batteries, fuel cells in households and combined heat and power stations are connected to the system. Contingency of all lines and transformers in this power grid is considered, so the number of contingencies is 17.

IEEE 39-bus power grid

The IEEE 39-bus power grid originates from [1]. It is a high voltage transmission grid with ten generators, as shown in Fig. 2-4. This grid is significantly larger than the other benchmark grids discussed above. This enables analysis and discussion on the scalability of different methods. Contingency of all non-islanding lines and transformers in this power grid is considered, so the number of contingencies is 46.

2-2 Load and generation data

To perform simulations on the different power grids, different realistic load and generation scenarios are considered, as is described in the following section.

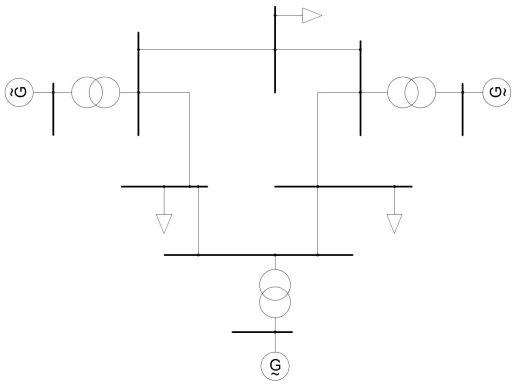

Figure 2-2: IEEE 9-bus power grid, adepted from [32].

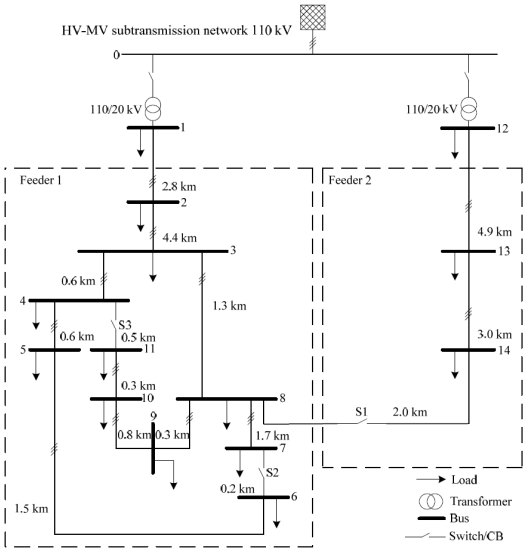

Figure 2-3: CIGRÉ MV power grid [9]

For the Middelharnis power grid, load and generation data is delivered by Stedin Netbeheer. The load profiles from [28] are used for all academic benchmark grids. These profiles are developed by NEDU, the Dutch association for energy data exchange, which is a joint initiative of the Dutch energy sector, including Stedin Netbeheer. The load profiles describe the hourly fraction of the total yearly electricity consumption for different types of connections. Standard practice at Stedin is to use the E1B load profile for residential connections and the E3A load profile for commercial and industrial connections. The E1B profile is based on 1401 series of Dutch smart meter data. The E3A profile is based on 3883 data series, made available to NEDU by balance responsible parties. Assuming an equal load profile for every residential or industrial load might not represent a realistic scenario. Especially when learning a process, these unnatural patterns could hinder learning the full complexity of the process. Therefore, a random adjustment of 10% is added to each different load. The reactive power load is determined by multiplying the active power load of each load by $0.2(\pm 0.1)$. This approach is stems from [13].

The generation profiles for the photovoltaic systems originate from the Dutch PV portal [10]. This portal delivers power profiles for photovoltaic systems based on the solar system design, modelling expertise of the Photovoltaic Materials and Devices group at Delft University of Technology and weather measurements of the Royal Netherlands Meteorological Institute (KNMI). A detailed description of this data portal is given in [36]. The generation profiles for the wind turbines in the Middelharnis power grid are given by Stedin Netbeheer.

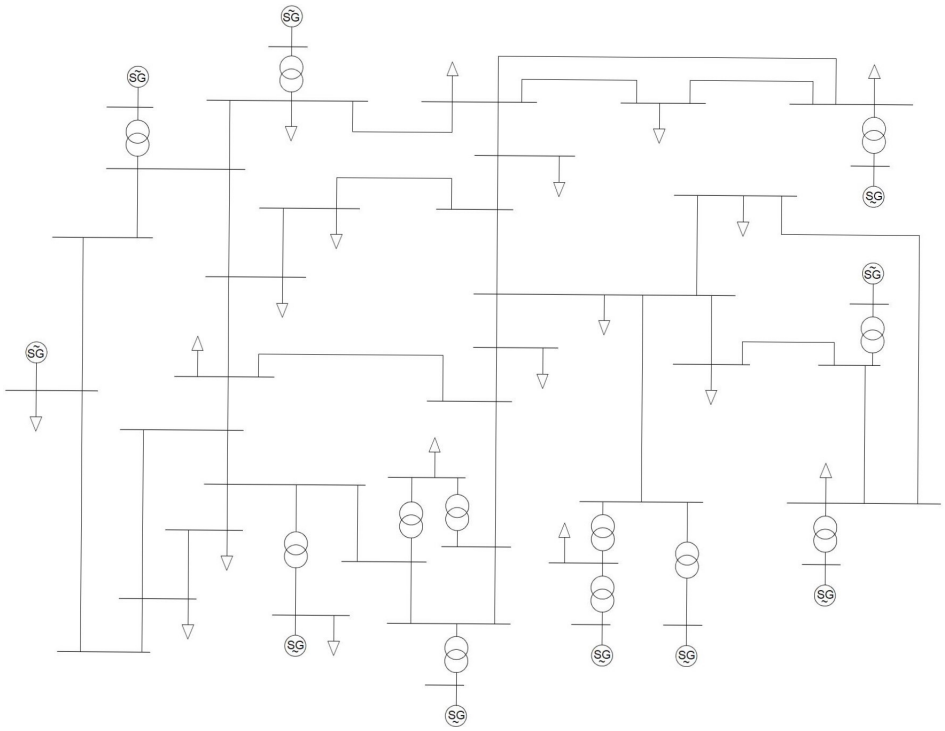

Figure 2-4: IEEE 39-bus power grid, adepted from [1].

Chapter 3

Preventive-corrective contingency control using differential evolution

Contingency control methods have been frequently studied in academic literature. In contingency control, a distinction is made between preventive and corrective control measures.

Corrective control is applied after a contingency has occurred. Preventive control is applied to the system prior to a potential contingency, to prevent or mitigate potential post-contingency constraint violations. Control actions are usually to be minimized, since they come at a cost. Corrective control has the advantage of being applied only when absolutely necessary. However, corrective control relies on two major assumptions [8]: (i) post-contingency constraint violations can be tolerated for a certain period of time, leaving enough time for the application of adequate corrective control actions and (ii) the system will remain stable in the period between contingency occurrence and the post-contingency steady-state operating point. The latter is called transient stability, which is mainly an issue with large-scale transmission grids. If either one of these assumptions does not hold, preventive control is a required alternative or addition to corrective control, even though it has the drawback that costly control action is applied regardless of the actual occurrence of a contingency. Due to this drawback, it is generally considered to be undesired to solve all possible post-contingent limit violations using preventive control. Thus, the combined use of preventive control and corrective control is preferred. This is called preventive-corrective control.

If preventive and corrective control methods can be decoupled, the preventive-corrective control does not differ significantly from preventive or corrective control. Separate monitoring and control algorithms can be implemented for both types of control. This is for example the case when the loading and voltage levels instantaneously after a contingency occurs are required to be within certain tight limits, but the time to apply corrective control actions and steer the system into a secure long-term grid situation is large enough for any required corrective control actions. Now, the preventive and corrective control actions can be computed separately, without any coupling between the two.

However, in some cases these different control actions might be coupled. For example, corrective control actions on the power output of generators might be limited in terms of their ramp

to prevent grid instability. The tolerated time to solve a limit violation in post-contingent grid state might therefore be exceeded if control actions are only applied in a corrective form. Therefore, preventive control should be applied. The amount of preventive control action influences the required corrective control actions for different contingencies. In these situations, the preventive and corrective control actions should be determined in a coupled manner.

Preventive-corrective control is characterized by the coupling between preventive and corrective control actions. One set of preventive control actions influences the sets of optimal corrective control actions for different contingencies. The studies in literature on preventive-corrective control have shown that this coupling requires extensive computational effort [8, 54, 55, 57], since multiple iterations are required between the preventive and corresponding corrective control actions to find optimal sets of these control actions. The study of [54] presents a hybrid method using an algorithm based on differential evolution (DE), which is a specific type of evolutionary algorithm. In this algorithm, preventive and corrective control actions are defined for a large population of offsprings. These population members are distinguished by their control variable space. After each iteration, the offspring population is updated according to specific evolutionary rules and the new offspring population is evaluated again. The evolutionary rules make sure that the new population is closer to the optimum then the previous. The contingency control problem is non-convex and might have multiple local minima. As long as the initial offspring population is sufficiently diverse, this algorithm is capable to escape local minima. A similar approach is used in [55], where a different parameter set is used to distinguish the different members of a population. In [57], the coupling between preventive and corrective control is quantified in a risk coordination parameter. The optimal value of this parameter is determined by performing a golden section searches on multiple parameter values until convergence. The parameter values are updated each iteration based on the previous golden section search. However, this golden section-based might struggle to escape local minima, since only two samples are used to define new values of the risk coordination parameter. This risk increases with an increasing number of control variables. The study in [8] focuses on the transient stability, where the main challenge in the case of Dutch distribution grid is the overloading of lines and transformers. Computation times for the above-mentioned methods range between 70 seconds for a small 14-bus system and 5527 seconds for a 118-bus system.

Given the above analysis, the most suitable preventive-corrective control method for this thesis is the method based on DE as proposed by [54] and [55]. The building blocks of the DE algorithm consist of performing contingency analysis and computing the optimal power flow (OPF). Therefore, these processes will first be described in Section 3-1 and Section 3-2. After this, the preventive-corrective contingency control method using DE will be discussed in detail in Section 3-3. To analyse the performance of this method, the method is tested on the case study using different design choices. The results of this testing are presented in Section 3-4 and conclusions are finally drawn in Section 3-5.

3-1 Contingency analysis

Contingency analysis is one of the important steps in contingency control. In this practice, the influence of possible contingencies on the power grid operation is analysed, given a particular loading scenario. In this particular case study, the contingency analysis method should be

able to determine which contingencies lead to limit violations in terms of voltage levels and the loading of remaining grid components.

Power flow computations form the basis for most contingency analysis methods. In power flow computations, all known loading and voltage data of the power grid is used to compute the power flows through all components of the grid. The used methods to solve the power flow problem are therefore discussed in Section 3-1-1. Using these power flow computation methods, two different classical contingency analysis methods are discussed in Section 3-1-2 and Section 3-1-3. Finally, the results of these methods on the case study are presented and discussed in Section 3-1-4 and conclusions are drawn in Section 3-1-5.

3-1-1 Power flow problem

The power flow is the network solution describing the active and real power flow and complex voltage value at each network bus. The power flow can be described by the following equations [61]:

$$P_i(\boldsymbol{V}, \boldsymbol{\theta}) = V_i \sum_{j=1}^{N} V_j \left(G_{ij} \cos\theta_{ij} + B_{ij} \sin\theta_{ij}\right) \tag{3-1}$$

$$Q_i(\boldsymbol{V}, \boldsymbol{\theta}) = V_i \sum_{j=1}^{N} V_j \left(G_{ij} \sin\theta_{ij} - B_{ij} \cos\theta_{ij}\right) \tag{3-2}$$

where V_i, θ_i, P_i and Q_i are the voltage magnitude and voltage angle and the active and reactive power flows at bus i, respectively. Furthermore, $\theta_{ij} = \theta_i - \theta_j$ is the voltage angle between bus i and j and G_{ij} and B_{ij} are the real and imaginary parts of the $[i, j]$ indices of the admittance matrix, given by:

$$Y_{ij} = G_{ij} + jB_{ij} = \begin{cases} -(g_{ij} + jb_{ij}), & \text{if } i \neq j \\ (g_i + jb_i) + \sum_{\substack{j=1 \\ j \neq i}}^{N} (g_{ij} + jb_{ij}), & \text{if } i = j \\ 0, & \text{if no connection exists} \end{cases} \tag{3-3}$$

This admittance matrix is constant for a particular power grid and describes the conductance and susceptance of the lines and transformers of the power grid.

Each bus has four variables (P_i, Q_i, θ_i and V_i) and two equations. Therefore, two variables have to be known for each bus to solve this set of equations. For load buses, the P and Q are known. For generator buses, the P and V are known. For swing buses, the θ and V are known. Since the power flow equations are non-linear, finding the solution for all variables is not straightforward. Two widely used algorithms to solve the power flow are discussed in the following sections.

Newton-Raphson method

The Newton-Raphson method is an accurate and widely used approach to solve the power flow equations. The following derivation originates from [61]. To this end, the following

mismatch equations are proposed, as presented in (3-1) and (3-2):

$$\Delta P_i = P_{is} - P_i = P_{is} - V_i \sum_{j=1}^{n} V_j \left(G_{ij} \cos\theta_{ij} + B_{ij} \sin\theta_{ij}\right) = 0 \tag{3-4}$$

$$\Delta Q_i = Q_{is} - Q_i = Q_{is} - V_i \sum_{j=1}^{n} V_j \left(G_{ij} \sin\theta_{ij} - B_{ij} \cos\theta_{ij}\right) = 0 \tag{3-5}$$

where P_{is} and Q_{is} are the known bus real and reactive power injections, respectively. Equation (3-4) has to hold for each PV and PQ bus and (3-5) has to hold for each PQ bus. It is assumed that bus n is a slack bus, buses 1 to m are PQ buses (where P_i and Q_i are known) and buses $(m+1)$ to $(n-1)$ are PV buses (where P_i and V_i are known). When these mismatch equations are expanded into Taylor series, the following first-order approximation can be obtained:

$$\begin{bmatrix} \boldsymbol{\Delta P} \\ \boldsymbol{\Delta Q} \end{bmatrix} = -J \begin{bmatrix} \boldsymbol{\Delta\theta} \\ \boldsymbol{\Delta V/V} \end{bmatrix} = - \begin{bmatrix} H & N \\ K & L \end{bmatrix} \begin{bmatrix} \boldsymbol{\Delta\theta} \\ V_D^{-1}\boldsymbol{\Delta V} \end{bmatrix} \tag{3-6}$$

where

$$\boldsymbol{\Delta P} = \begin{bmatrix} \Delta P_1 \\ \Delta P_2 \\ \vdots \\ \Delta P_{n-1} \end{bmatrix} \tag{3-7}$$

$$\boldsymbol{\Delta Q} = \begin{bmatrix} \Delta Q_1 \\ \Delta Q_2 \\ \vdots \\ \Delta Q_m \end{bmatrix} \tag{3-8}$$

$$\boldsymbol{\Delta\theta} = \begin{bmatrix} \Delta\theta_1 \\ \Delta\theta_2 \\ \vdots \\ \Delta\theta_{n-1} \end{bmatrix} \tag{3-9}$$

$$\boldsymbol{\Delta V} = \begin{bmatrix} \Delta V_1 \\ \Delta V_2 \\ \vdots \\ \Delta V_m \end{bmatrix} \tag{3-10}$$

$$V_D = \mathrm{diag}(V_1, V_2, ..., V_m) \tag{3-11}$$

H is an $(n-1)\times(n-1)$ matrix, and each element with index (i,j) is described by $H_{ij} = \frac{\partial \Delta P_i}{\partial \theta_j}$.
N is an $(n-1)\times m$ matrix, and each element with index (i,j) is described by $N_{ij} = V_j \frac{\partial \Delta P_i}{\partial V_j}$.
K is an $m \times (n-1)$ matrix, and each element with index (i,j) is described by $K_{ij} = \frac{\partial \Delta Q_i}{\partial \theta_j}$.
L is an $m \times m$ matrix, and each element with index (i,j) is described by $L_{ij} = V_j \frac{\partial \Delta Q_i}{\partial V_j}$.

For $i \neq j$, the expressions for these matrices are given by

$$\begin{aligned} H_{ij} &= -V_i V_j \left(G_{ij} \sin\theta_{ij} - B_{ij} \cos\theta_{ij}\right) \\ N_{ij} &= -V_i V_j \left(G_{ij} \cos\theta_{ij} - B_{ij} \sin\theta_{ij}\right) \\ K_{ij} &= V_i V_j \left(G_{ij} \cos\theta_{ij} - B_{ij} \sin\theta_{ij}\right) \\ L_{ij} &= -V_i V_j \left(G_{ij} \sin\theta_{ij} - B_{ij} \cos\theta_{ij}\right) \end{aligned} \tag{3-12}$$

For $i = j$, the expressions are given by

$$\begin{aligned} H_{ii} &= V_i^2 B_{ii} + Q_i \\ N_{ii} &= -V_i^2 G_{ii} - P_i \\ K_{ii} &= V_i^2 G_{ii} - P_i \\ L_{ii} &= V_i^2 B_{ii} - Q_i \end{aligned} \tag{3-13}$$

Now, given input data for each bus, the bus admittance matrix of the network and some initial bus voltage and angle values, the power mismatch equations (3-4) and (3-5) can be solved by computing the Jacobian matrix J, using the initial bus voltage and angle values. This Jacobian is used to solve (3-6) for $\boldsymbol{\Delta\theta}$ and $\boldsymbol{\Delta V}$, after which the bus voltages of PQ buses and bus angles of all buses are updated according to

$$\begin{aligned} V_i^{(k+1)} &= V_i^{(k)} + \Delta V_i^{(k)} \\ \theta_i^{(k+1)} &= \theta_i^{(k)} + \Delta\theta_i^{(k)} \end{aligned} \tag{3-14}$$

where k is the iteration number. Now, it can be checked whether the algorithm has converged, i.e. $\max|\Delta P_i|$ and $\max|\Delta Q_i|$ are below certain thresholds. Otherwise, the computations are iterated by computing the Jacobian matrix again, and so forth.

This algorithm requires computation of the Jacobian matrix and its inverse for each iteration and these iterations are required for each contingency when performing contingency analysis. An application of this method is shown in [38]. When assessing larger power grids, the amount of contingencies to consider increases, as well as the computational effort to compute the Jacobian matrix and its inverse. This results in a large computational burden. The greater part of this burden is caused by the computation of the Jacobian matrix. Reducing the computational time is therefore mainly focused on this Jacobian matrix. A means to do this is by decoupling the active and reactive power changes, which is demonstrated in the following section.

Fast decoupled load flow method

A commonly used power flow computation technique is the fast decoupled load flow (FDLF) [43]. For high voltage systems, the resistance to reactance ratio R/X is generally low ($\ll 1$). This means that the influence of V_j on P_i is relatively small compared to the influence of θ_j on P_i while the influence of V_j on Q_i is relatively large compared to that of θ_j on Q_i. Therefore, the following assumptions are made:

$$\frac{\partial \Delta P_i}{\partial V_j} \approx 0 \tag{3-15}$$

$$\frac{\partial \Delta Q_i}{\partial \theta_j} \approx 0 \tag{3-16}$$

This means that (3-6) is reduced to

$$\begin{bmatrix} \boldsymbol{\Delta P} \\ \boldsymbol{\Delta Q} \end{bmatrix} = -\begin{bmatrix} H & 0 \\ 0 & L \end{bmatrix} \begin{bmatrix} \boldsymbol{\Delta\theta} \\ V_D^{-1}\boldsymbol{\Delta V} \end{bmatrix} \tag{3-17}$$

Now, the real and reactive power mismatch is decoupled and can be used separately to compute the voltage magnitude and angle, respectively. Additional assumptions can be made to simplify (3-17) even further. The difference of voltage angles of two ends in a line (θ_{ij}) is generally small. Therefore, we have

$$\begin{aligned} \cos\theta_{ij} = \cos\left(\theta_i - \theta_j\right) &\approx 1 \\ G_{ij}\sin\theta_{ij} &\ll B_{ij} \end{aligned} \tag{3-18}$$

We can now rewrite H_{ij} and L_{ij} of (3-12) for $i \neq j$ as:

$$H_{ij} = V_i V_j B_{ij} \quad i,j = 1,2,\ldots,n-1 \tag{3-19}$$

$$L_{ij} = V_i V_j B_{ij} \quad i,j = 1,2,\ldots,m \tag{3-20}$$

If we use the assumptions of (3-18) and assume a flat voltage profile, meaning that two adjacent buses have the same voltage level, i.e. $V_i = V_j$, then H_{ii} and L_{ii} are defined by

$$H_{ii} = B_{ii}V_i^2 - \sum_{j=1}^{N} V_i^2 B_{ij} = V_i^2\left(B_{ii} - \sum_{j=1}^{N} B_{ij}\right) \tag{3-21}$$

$$L_{ii} = B_{ii}V_i^2 + \sum_{j=1}^{N} V_i^2 B_{ij} = V_i^2\left(B_{ii} + \sum_{j=1}^{N} B_{ij}\right) \tag{3-22}$$

From (3-3) we know that $B_{ij} = -b_{ij}$ for $i \neq j$ and $B_{ij} = b_i + \sum_{\substack{j=1 \\ j\neq i}}^{N} b_{ij}$ for $i = j$. Therefore, (3-21) and (3-22) can be rewritten into

$$H_{ii} = V_i^2\left(B_{ii} + \sum_{\substack{j=1 \\ j\neq i}}^{N} b_{ij} - b_i - \sum_{\substack{j=1 \\ j\neq i}}^{N} b_{ij}\right) = V_i^2\left(B_{ii} - b_i\right) \tag{3-23}$$

$$L_{ii} = V_i^2\left(B_{ii} - \sum_{\substack{j=1 \\ j\neq i}}^{N} b_{ij} + b_i + \sum_{\substack{j=1 \\ j\neq i}}^{N} b_{ij}\right) = V_i^2\left(B_{ii} + b_i\right) \tag{3-24}$$

We know that B_{ii} is generally much larger than b_i, since b_i describes the effect of the line charging, which is generally relatively small. Therefore, all elements of H and L, including the case where $i = j$, can be approximated by

$$H_{ij} = V_i V_j B_{ij} \quad i,j = 1,2,\ldots,n-1 \tag{3-25}$$

$$L_{ij} = V_i V_j B_{ij} \quad i,j = 1,2,\ldots,m \tag{3-26}$$

and (3-17) can be rewritten into

$$V_{D1}^{-1}\boldsymbol{\Delta P} = B' V_{D1}\boldsymbol{\Delta\theta} \tag{3-27}$$

$$V_{D2}^{-1}\boldsymbol{\Delta Q} = B''\boldsymbol{\Delta V} \tag{3-28}$$

where

$$V_{D1} = \begin{bmatrix} V_1 & & & \\ & V_2 & & \\ & & \ddots & \\ & & & V_{n-1} \end{bmatrix} \tag{3-29}$$

$$V_{D2} = \begin{bmatrix} V_1 & & & \\ & V_2 & & \\ & & \ddots & \\ & & & V_m \end{bmatrix} \tag{3-30}$$

and B' and B'' only consist of B_{ij} values of the admittance matrix. For full derivation, consult [61]. The right-hand side V_{D1} in (3-27) is now assumed to be identity, simplifying the equation to

$$V_{D1}^{-1}\boldsymbol{\Delta P} = B'\boldsymbol{\Delta\theta} \tag{3-31}$$

Now the iteration depicted in Fig. 3-1 is executed, where (3-4) and (3-5) are used to compute $\boldsymbol{P}$ and $\boldsymbol{Q}$, after solving (3-31) and (3-28) and checking their convergence.

Executing one iteration of this FDLF algorithm is computationally simple compared to an iteration of the Newton-Raphson method. However, the convergence rate per iteration is lower, due to the assumptions that are made. The decrease of the convergence rate is dependent on the validity of the assumptions for the specific power flow scenario. When the assumptions are reasonable, the FDLF delivers a lower convergence time as was discussed in [42]. Since the power flow equations are non-convex, it is not guaranteed that the FDLF algorithm will converge to the global optimum. Again, the likelihood of convergence to the global optimum decreases when the validity of the assumptions worsens. As presented in [6], the error on the results of the FDLF method is well below 1% on average when the assumptions are generally adhered to. The most crucial assumption when applying the FDLF to distribution power systems is the assumption of low R/X ratio, since this is not valid for most distribution power systems. In [47], it is shown that this method does not converge for the 14-, 30- and 57-bus IEEE test systems, which are really comparable to the case study of this thesis in terms of their R/X ratio. However, several efforts have successfully improved the convergence rate and accuracy of FDLF for lower voltage power systems with larger R/X ratio [16, 27, 31, 33, 47]. The most important variants of the FDLF method are described in [47]. Adjustments are made to the B' and B'' matrices, to account for the existing coupling between the active and reactive power. It is found by the authors of the paper that BX variant usually delivers the best performance. In this variant, the B' and B'' matrices are computed as follows:

$$\begin{aligned} B'_{ij} &= -\frac{x_{ij}}{r_{ij}^2 + x_{ij}^2} \\ B'_{ii} &= \sum_{j \neq i} \frac{x_{ij}}{r_{ij}^2 + x_{ij}^2} \\ B''_{ij} &= -\frac{1}{x_{ij}} \\ B''_{ii} &= -\sum_{j \neq i} B''_{ij} \end{aligned} \tag{3-32}$$

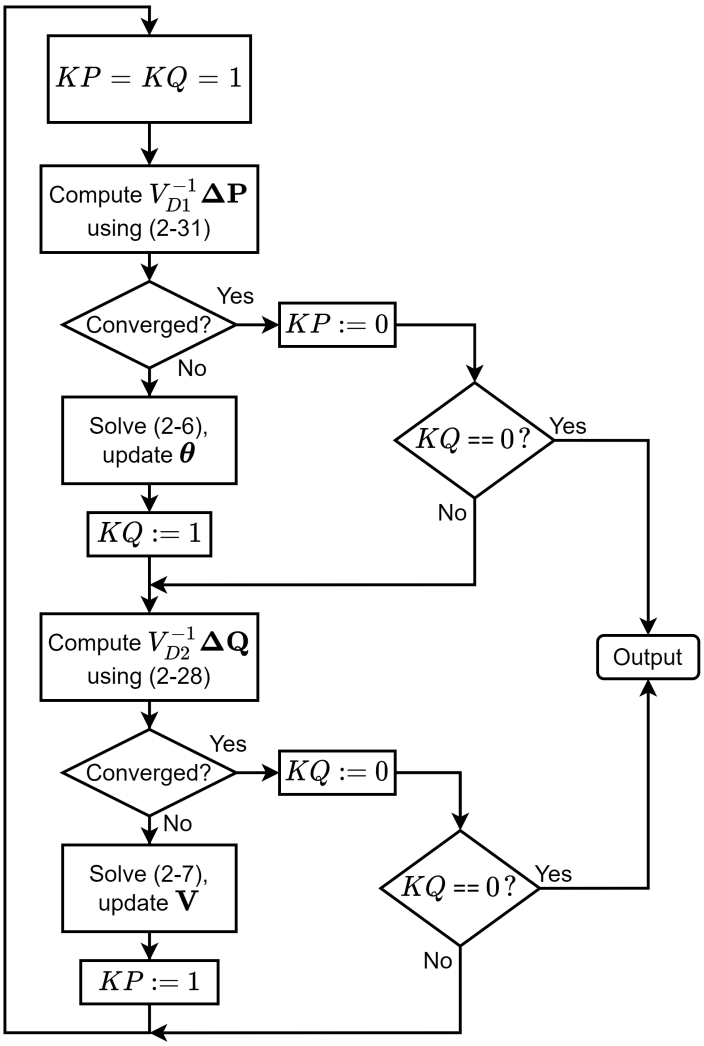

Figure 3-1: Fast decoupled load flow iteration scheme, adepted from [43].

where r_{ij} and x_{ij} are the resistance and reactance between bus i and j, respectively. In [47] and [27], it is shown that this BX variant is very capable to compute the power flow of distribution grids with comparable or even higher R/X ratios with respect to the systems in this case study. It might take a few more iterations compared to the Newton-Raphson method as described above, but due to the simplicity of the iterations, the computational time to converge is similar for smaller grids. For larger grids, the BX FDLF-method delivers superior computational times. In this research, the standard Newton-Rapshon method is used, since only relatively small grids are used in the case study. However, the FDLF method serves as a basis for the contingency analysis method based on line outage distribution factors, which will be discussed later in Section 3-1-3.

3-1-2 Complete AC power flow method

Automatic contingency selection is introduced by Ejebe et al. in [14], using the complete AC power flow method. This method iterates through all contingencies, computes the AC power flow using the Newton-Raphson method and detects any constraint violations. In later studies, line overloads, load loss, frequency deviation and other parameters were also included in the performance index. Of course, other power flow computation methods can also be used, depending on the suitability of the different methods for the particular case study. For example, the FDLF method is used in [48], where transmission power system models are used as case study. In [19], the FDLF method is also used.

In this research, the Newton-Raphson method will be used to solve the power flow equations. This power flow method is very versatile, since it is suitable for different network configurations and voltage levels. Moreover, the main focus of this study is on distribution power grids, for which the FDLF is generally known not to add significant improvement in computational efficiency, as is discussed above.

After the power flow computation, a contingency is determined to be critical or non-critical based on the voltage levels of buses and the loading percentages of lines and transformers. The voltage levels follow directly from the power flow computations. Using the admittance data and voltage results, the power flow from bus i to bus j can be defined using [24]:

$$P_{ij} = V_i V_j |Y_{ij}| \cos(\theta_{ij} - \phi_{ij}) - V_i^2 |Y_{ij}| \cos \phi_{ij} \tag{3-33}$$

$$Q_{ij} = V_i V_j |Y_{ij}| \sin(\theta_{ij} - \phi_{ij}) - V_i^2 |Y_{ij}| \sin \phi_{ij} \tag{3-34}$$

$$\tag{3-35}$$

where $|Y_{ij}|$ is the absolute value of the admittance between bus i and j and ϕ_{ij} is the corresponding complex angle. Now, the apparent power can be defined by:

$$S_{ij} = \sqrt{P_{ij}^2 + Q_{ij}^2} \tag{3-36}$$

and the current flow is defined as:

$$I_{ij} = |S_{ij}/V_{ij}| \tag{3-37}$$

the loading l on the component is now determined as follows:

$$l = I_{ij}/I_{ij,\text{nom}} \cdot 100\% \tag{3-38}$$

where $I_{ij,\text{nom}}$ is the nominal current of the component.

In the complete AC power flow contingency analysis method, the power flow computations and voltage and loading violations check is performed for each possible contingency. The output of the algorithm is a list of critical contingencies for this current grid state.

3-1-3 Line outage distribution factors

Instead of completely solving the power flow equations, approximated linearized methods can also be used to perform contingency ranking and selection. A well-known instrument to approximate the post-contingency power flow is the line outage distribution factor (LODF). This factor is given by [51]:

$$\text{LODF}_{\ell,k} = \frac{\Delta f_\ell}{f_k^{(0)}} \tag{3-39}$$

where

$\text{LODF}_{\ell,k}$ = line outage distribution factor when monitoring line ℓ after an outage on line k
Δf_ℓ = change in MW flow on line ℓ
$f_k^{(0)}$ = original flow on line k before it was contingent.

If these LODFs are known, the flow $\hat{f}_\ell$ on any line ℓ of the power system after outage of component k can be determined by:

$$\hat{f}_\ell = f_\ell^{(0)} + \Delta f_\ell = f_\ell^{(0)} + \text{LODF}_{\ell,k} f_k^{(0)} \tag{3-40}$$

without requiring any further power flow equations.

It should be noted that this LODF-based contingency analysis method is by definition not able to analyse voltage violations due to any contingencies. This poses an important limitation on this contingency analysis method.

The LODFs can be determined from only the admittance data of the power grid, as is done in [49]. In this paper, contingency analysis using this method is performed. The contingency analysis requires the pre-contingency power flow data and the LODFs of the power grid. The method is considerably faster than the full AC power flow method using the Newton-Raphson or FDLF power flow method. However, nodal voltage violations can not be assessed using this method and there is a fault range of 0.2 to 5% compared to the before-mentioned methods. The derivation of the LODF values based on the admittance data originates from [51] and is given in the following sections.

Derivation of LODFs based on PTDFs

The contingency of any component k, placed between buses i and j, can be represented by power injections Δf at buses i and j, as is visualised in Fig. 3-2.

The power injections Δf_i and Δf_j represent the outage of line k if and only if

$$\Delta f_i = \tilde{f}_k \tag{3-41}$$

$$\Delta f_j = -\tilde{f}_k \tag{3-42}$$

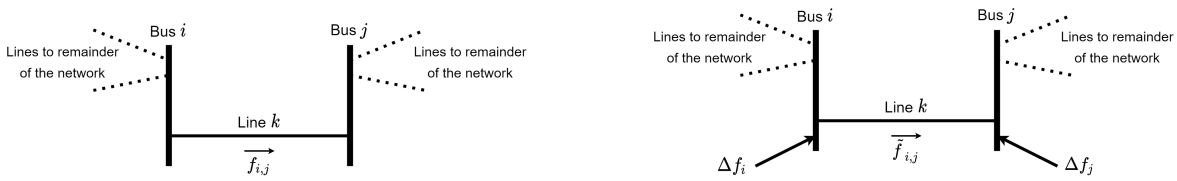

(a) Pre-contingent situation

(b) Post-contingent situation

Figure 3-2: Line contingency representation using power injections, adepted from [51].

We now introduce the power transfer distribution factor (PTDF), described by:

$$\text{PTDF}_{i,j,k} = \frac{\Delta f_k}{\Delta f_{i,j}} \tag{3-43}$$

where Δf_k is the change of power flow through component k, due to $\Delta f_{i,j}$, a transfer of power input from bus i to bus j. Using this factor, the following flow can be computed:

$$\tilde{f}_k = f_k^{(0)} + \text{PTDF}_{i,j,k}\Delta f_{i,j} \tag{3-44}$$

where $f_k^{(0)}$ is the flow through component k prior to the power transfer and $\tilde{f}_k$ is the flow through component k after the power transfer $\Delta f_{i,j}$ from bus i to bus j. In the case of Fig. 3-2, from (3-41) and (3-42), we know that $\Delta f_{i,j} = \tilde{f}_k$, which gives:

$$\tilde{f}_k = f_k^{(0)} + \text{PTDF}_{i,j,k}\tilde{f}_{i,j} \tag{3-45}$$

which can be rewritten into:

$$\tilde{f}_k = \left(\frac{1}{1 - \text{PTDF}_{i,j,k}}\right) f_k^{(0)} \tag{3-46}$$

The change in flow on line ℓ from s to j now logically follows as:

$$\Delta f_\ell = \text{PTDF}_{i,j,\ell}\tilde{f}_{i,j} = \text{PTDF}_{i,j,\ell}\tilde{f}_k = \text{PTDF}_{i,j,\ell}\left(\frac{1}{1 - \text{PTDF}_{i,j,k}}\right) f_k^{(0)} \tag{3-47}$$

Substituting f_ℓ from (3-47) into (3-40), it follows that:

$$\text{LODF}_{l,k} = \text{PTDF}_{i,j,\ell}\left(\frac{1}{1 - \text{PTDF}_{i,j,k}}\right) \tag{3-48}$$

It is hereby demonstrated that the LODFs can be determined from PTDFs only.

Approximated PTDFs based on admittance data

If the PTDFs can be approximated based on admittance data, we are able to perform contingency analysis for all contingencies using only the pre-contingent power flow and the admittance data of the power grid. To do this, we use (3-27) and assume the voltage levels

of all buses to be equal to 1. All calculations are done in a per-unit system, which means all different voltage levels are normalised. Furthermore, the power grids of main importance are distribution power grids, which are generally well-balanced in terms of voltage levels. Therefore, V_{D1} and V_{D1}^{-1} are assumed to be identity matrices. Equation (3-27) then reduces to:

$$\boldsymbol{\Delta P} = B' \boldsymbol{\Delta \theta} \tag{3-49}$$

The phase angle changes due to a power transfer from bus i to bus j can now be approximated by:

$$\boldsymbol{\Delta \theta} = [X] \boldsymbol{\Delta P_{i,j}} \tag{3-50}$$

where $\boldsymbol{\Delta \theta}$ is the vector consisting of phase angle changes for each bus, $[X] = (B')^{-1}$ and $\boldsymbol{\Delta P_{i,j}}$ is a vector with all zeros, expect a $+1$ at index i and -1 at index j. The phase angle changes of bus m and n due to power transfer between buses i and j are now approximated by:

$$\Delta\theta_m = X_{mi} - X_{mj} \tag{3-51}$$

$$\Delta\theta_n = X_{ni} - X_{nj} \tag{3-52}$$

The linear power flow equation is now derived from (3-1), by assuming that all bus voltages are 1, the assumptions from (3-18) and $\sin\theta_i - \theta_j \approx \theta_i - \theta_j$, which holds for small angles. The linear power flow is now:

$$P_m = \sum_{j=1}^{N} B_{mn}(\theta_m - \theta_n) \tag{3-53}$$

Using this, the change of flow on line k from m to n is now:

$$\Delta f_k = B_k(\Delta\theta_m - \Delta\theta_n) = B_k((X_{mi} - X_{mj}) - (X_{ni} - X_{nj})) \tag{3-54}$$

The change of power flow Δf_k and the transferred power $\Delta P = 1$ can now be substituted into (3-43) to get:

$$PTDF_{i,j,k} = B_k((X_{mi} - X_{mj}) - (X_{ni} - X_{nj})) \tag{3-55}$$

It is now shown that the PTDF values can be approximated from only admittance data, assuming that the linear power flow is a reasonable approximation of the non-linear power flow and assuming a flat voltage profile. Using the BX variant of the matrix B', as described in (3-32), is supposed to increase the accuracy of this method for higher R/X systems, where the default linear power flow approximation might not be sufficient.

In [35], this LODF-based method is used to perform contingency analysis. It is shown in this research that this method can lead to large errors, compared to the full AC power flow method and an artificial neural network method. However, the research also shows that the computational efficiency of this method is superior.

3-1-4 Contingency analysis results on case study

To analyse the results of the full AC power flow method and the LODF-based method, contingency analysis using these methods is performed on the Stedin Middelharnis power grid and all proposed academic benchmark power grids. The full AC power flow method is the most accurate method and will therefore be considered 100% accurate. Naturally, the accuracy of this method is depending on the accuracy of the admittance and nominal current data and the input bus data, consisting of voltages and load and generation powers. In this research, this data is assumed to be correct. Therefore, the accuracy of the LODF-based method will be compared to the output of the full AC power flow method. The first accuracy measure is the percentage of contingencies which are accurately identified as being safe, alarming or critical. However, for the application of contingency control, the insecure contingency cases are of main interest. To ensure safe grid operation, all insecure cases should be considered when performing contingency control in a later stage. Therefore, the percentage of unidentified insecure cases is analysed for all networks.

Accuracy of LODF-based method

The results of the LODF-based method are shown in Table 3-1. It can be observed that the accuracy for this method is larger than 90% for all power grids, except the IEEE 9-bus grid. This deviation can be explained from the limitations of the LODF method. First of all, the LODF-based method is not able to deal with islanding. This means that a contingency might cut off a certain part of the grid from the remainder. When performing full AC power flow computations, the power flow of the remainder of the grid can be computed without the part of the grid which is disconnected. However, the LODF-based method computes the new power flows directly from the pre-contingent flow, using the LODF factors. This means that there is no way to consider the islanded situation and therefore the fundamental change in power flow, other than recognizing the islanded situation and compute a new power flow for this particular islanded situation. However, this would deteriorate the computational benefit of the LODF-based method for this particular contingency. The IEEE 9-bus power grid is the smallest sized grid in this case study. Therefore, the influence of disconnected generators from the grid is the largest for this grid. Furthermore, the LODF-based method relies on the linear DC power flow. This means that congestion due to reactive power can not be considered. In the IEEE 9-bus power grid, critical contingencies often stem from the overloaded transformers, due to the increased reactive power. These two factors also explain why 100% of the insecure cases is unidentified for the IEEE 9-bus system. All insecure cases are due to the disconnection of a generator due to the contingency or due to reactive power loading on transformers, or both. It therefore follows that this LODF-based method is not suitable for this grid. The Middelharnis power grid has no contingencies which disconnect any parts of the power grid from the remainder. This is the reason why the LODF-based method has the best performance for this power grid.

Computational efficiency comparison

For the complete AC power flow method, the computational time to perform the contingency analysis is of foremost interest. This data is presented and compared to the evaluation time of

Grid	Accuracy (%)	Unidentified insecure cases (%)	Evaluation time (s)
IEEE 9-bus	66.78	100	0.031
Middelharnis	90.34	6.32	0.052
CIGRÉ MV	97.95	9.78	0.052
IEEE 39-bus	90.39	23.62	0.179

Table 3-1: LODF-based method contingency analysis results

the LODF-based method in Table 3-2. Evaluating the neural networks is considerably faster compared to the full AC power flow computation using Newton-Raphson. The LODF-based method performs 2 to 10 times faster than the full AC power flow method. With increasing power grid size, the benefit of the LODF-based method compared to the full AC power flow method increases. This means that for larger power grids, where the computational complexity of contingency analysis is a problem, the value of the LODF-based method increases.

Grid	Buses	Contingencies	Evaluation time (s)	
			Full AC power flow	LODF
IEEE 9-bus	9	6	0.059	0.031
Middelharnis	9	12	0.33	0.052
CIGRÉ MV	15	17	0.22	0.052
IEEE 39-bus	39	46	1.80	0.18

Table 3-2: Comparison of evaluation time for LODF and full AC power flow methods.

3-1-5 Conclusions on contingency analysis methods

The LODF-based method delivers improved computational efficiency compared to the full AC power flow method for the considered case study grids. However, the inaccuracy of the LODF method will cause critical contingencies to be neglected and might therefore very well steer the system into a critical state. Furthermore, the LODF-based method is not able to detect voltage violations, which limits the capabilities of the contingency control method when this analysis method is used. The preferred contingency analysis method for the DE-based contingency control method of this chapter is therefore the full AC power flow method.

3-2 Optimal power flow

The second important process in the preventive-corrective contingency control is the computation of the OPF. This OPF problem is basically an extension of the power flow problem,

where control parameters, a cost function and (in)equality constraints are added to the problem. Now, the challenge is to determine the optimal control variables which minimizes the cost function and satisfies the (in)equality constraints, such as component loading limits and voltage level limits. Typical objectives to be minimized fuel cost, generator curtailment and switching actions. Control variables are typically the demand or supply of energy, referred to in literature as load shedding and generation curtailment and switching actions. The general OPF problem is presented in [59] as follows:

$$\begin{aligned}
&\min F && && \text{(3-56a)}\\
&\text{subject to} && P_i(\boldsymbol{V},\boldsymbol{\theta}) = P_{G,i} + P_{CG,i} - P_{D,i} && \text{(3-56b)}\\
& && Q_i(\boldsymbol{V},\boldsymbol{\theta}) = Q_{G,i} - Q_{D,i} && \text{(3-56c)}\\
& && P_{CG,i,\min} \leq P_{CG,i} \leq P_{CG,i,\max} && \text{(3-56d)}\\
& && V_{i,\min} \leq V_i \leq V_{i,\max} && \text{(3-56e)}\\
& && I_{k,\min} \leq I_k(\boldsymbol{V},\boldsymbol{\theta}) \leq I_{k,\max} && \text{(3-56f)}\\
& && && \text{(3-56g)}
\end{aligned}$$

where

- F: the objective function, of which the details will be discussed later in this section
- $P_{G,i}$: the combined active power output of all uncontrollable generators at bus i
- $P_{CG,i}$: the combined active power output of all controllable generators at bus i
- $Q_{G,i}$: the combined reactive power output of all uncontrollable generators at bus i
- $P_{D,i}$: the combined active power of all loads at bus i
- $Q_{D,i}$: the combined reactive power of all loads at bus i
- $\boldsymbol{V}$: the vector of voltage levels for all buses i
- $\boldsymbol{\theta}$: the vector of voltage angles for all buses i
- $P_{G,i}$: the power output of the controllable generator at bus i
- I_l: the current flow through line l

and all variables with subscript max or min are the maximum and minimum values. Equations (3-56b) and (3-56c) are the power flow equations as described in Section 3-1-1.

Before solving the above OPF problem, we first define the state variables $\boldsymbol{x}$ as:

$$\boldsymbol{x} = \begin{bmatrix} \left.\begin{matrix}\theta\\ V\end{matrix}\right\} & \text{on each } PQ \text{ bus} \\ \left.\begin{matrix}\theta\\ Q_G\end{matrix}\right\} & \text{on each } PV \text{ bus} \\ \left.\begin{matrix}P_G\\ Q_G\end{matrix}\right\} & \text{on reference bus} \end{bmatrix} \tag{3-57}$$

and all known, specified variables $\boldsymbol{y}$ as

$$\boldsymbol{y} = \begin{bmatrix} \left.\begin{matrix} \theta_{\text{ref}} \\ V_{\text{ref}} \end{matrix}\right\} \text{on reference bus} \\ \left.\begin{matrix} P_D \\ P_G \\ Q_D \\ Q_G \end{matrix}\right\} \text{on each } PQ \text{ bus} \\ \left.\begin{matrix} P_G \\ P_D \\ V \end{matrix}\right\} \text{on each } PV \text{ bus} \end{bmatrix} \tag{3-58}$$

Of all variables in $\boldsymbol{y}$, only the P_G variables of the buses with controllable generators connected are adjustable. All other variables are fixed, such as the load and generation values P and Q at each load bus. Vector $\boldsymbol{y}$ can therefore be partitioned into a vector $\boldsymbol{u}$ of control parameters and a vector $\boldsymbol{w}$ of fixed parameters:

$$\boldsymbol{y} = \begin{bmatrix} \boldsymbol{u} \\ \boldsymbol{w} \end{bmatrix} \tag{3-59}$$

The parameters of $\boldsymbol{w}$ may vary over time, but are known for any moment and time and remain constant during the optimisation process. These constant values are therefore omitted in the notation in the following derivation.

Different choices can be made for the objective function F. With a linear cost function, the power output generator with the largest influence on the voltage or current limit violation will always be used to alleviate the limit violation. This will lead to the most efficient optimisation from an energetic point of view. However, in reality, it might be desirable to use multiple generators to alleviate a limit violation, even though not all generators have equal influence. Different generators are generally owned by different entities and therefore it might be favorable to spread the generator output reduction over different generators to prevent a large power output reduction of one particular generator. The objective function should be carefully selected for each particular situation based on the agreements with the owners of the controllable generators. The same holds for the cost parameters for different generators. These should be connected to the compensation costs owed to generator owners in case of power output limitation. In this case study, a quadratic objective function is selected and the cost parameter is equal for all controllable generators. This leads to the following objective function:

$$F = \sum_{j \in S_{\text{CG}}} c_j \left(P_{G,j}^{(0)} - P_{G,j} \right)^2 \tag{3-60}$$

where S_{CG} is the set of buses with controllable generators, c_j is the cost parameter for the reduction of power output of generator j, which is constant for all j.

Now, the equality and inequality constraints are rearranged to fit the standard formulation

of optimisation problems:

$$W_{P,i} = V_i \sum_{j=1}^{N} V_j \left(G_{ij}\cos\theta_{ij} + B_{ij}\sin\theta_{ij}\right) - P_{G,i} + P_{D,i} = 0 \tag{3-61a}$$

$$W_{Q,i} = V_i \sum_{j=1}^{N} V_j \left(G_{ij}\sin\theta_{ij} - B_{ij}\cos\theta_{ij}\right) - Q_{G,i} + Q_{D,i} = 0 \tag{3-61b}$$

$$W_{G,\max,i} = P_{G,i} - P_{G,i,\max} \leq 0 \tag{3-61c}$$

$$W_{G,\min,i} = P_{G,i,\min} - P_{G,i} \leq 0 \tag{3-61d}$$

$$W_{V,\max,i} = V_i - V_{i,\max} \leq 0 \tag{3-61e}$$

$$W_{V,\min,i} = V_{i,\min} - V_i \leq 0 \tag{3-61f}$$

$$W_{I,\max,k} = I_k(\boldsymbol{x}) - I_{k,\max} \leq 0 \tag{3-61g}$$

$$W_{I,\min,k} = I_{k,\min} - I_k(\boldsymbol{x}) \leq 0 \tag{3-61h}$$

Since this OPF will be solved in an iterative manner, the constraints on the power output of the controllable generators can be satisfied by clipping the new control values to the specified minimum and maximum values, as is suggested and demonstrated in [60]. Therefore, there is no need to include the constraints (3-61c) and (3-61d) explicitly in the following mathematical derivation of the OPF. We can stack all remaining inequality constraints into vector g:

$$\boldsymbol{g}(\boldsymbol{x},\boldsymbol{u}) = \begin{bmatrix} \boldsymbol{W}_{\boldsymbol{V,\max}}^{\mathsf{T}} & \boldsymbol{W}_{\boldsymbol{V,\min}}^{\mathsf{T}} & \boldsymbol{W}_{\boldsymbol{L,\max}}^{\mathsf{T}} & \boldsymbol{W}_{\boldsymbol{L,\min}}^{\mathsf{T}} \end{bmatrix}^{\mathsf{T}} \tag{3-62}$$

Now, the Lagrangian (L), the augmented unconstrained objective function with Lagrange multipliers ($\boldsymbol{\lambda}$) for equality constraints and penalty functions (p) for inequality constraints, is introduced:

$$L(\boldsymbol{x},\boldsymbol{u},\boldsymbol{\lambda}) = F + \boldsymbol{\lambda}^{\mathsf{T}} \begin{bmatrix} \boldsymbol{W_P}(\boldsymbol{x},\boldsymbol{u}) \\ \boldsymbol{W_Q}(\boldsymbol{x},\boldsymbol{u}) \end{bmatrix} + p(\boldsymbol{g}(\boldsymbol{x},\boldsymbol{u})) \tag{3-63}$$

Penalty function p should be 0 if $g_i = 0$ for all i and should be large otherwise. Furthermore, the function should have a continuous derivative, to be able to perform Newton's method. We therefore introduce the following penalty function:

$$p(\boldsymbol{g}(\boldsymbol{x},\boldsymbol{u})) = \beta \sum_{i=1}^{m} \max(0, g_i(\boldsymbol{x},\boldsymbol{u}))^2, \quad \beta \gg 1 \tag{3-64}$$

The Lagrangian optimisation problem is now defined as:

$$\min_{\boldsymbol{x},\boldsymbol{u},\boldsymbol{\lambda}} L(\boldsymbol{x},\boldsymbol{u},\boldsymbol{\lambda}) \tag{3-65}$$

At the optimum, the following conditions hold by definition:

$$\frac{\partial L(\boldsymbol{x},\boldsymbol{u},\boldsymbol{\lambda})}{\partial \boldsymbol{\lambda}} = \begin{bmatrix} \boldsymbol{W_P}(\boldsymbol{x},\boldsymbol{u}) \\ \boldsymbol{W_Q}(\boldsymbol{x},\boldsymbol{u}) \end{bmatrix} = \mathbf{0} \tag{3-66}$$

$$\frac{\partial L(\boldsymbol{x},\boldsymbol{u},\boldsymbol{\lambda})}{\partial \boldsymbol{x}} = \frac{\partial F}{\partial \boldsymbol{x}} + \begin{bmatrix} \frac{\partial \boldsymbol{W_P}(\boldsymbol{x},\boldsymbol{u})}{\partial \boldsymbol{x}} \\ \frac{\partial \boldsymbol{W_Q}(\boldsymbol{x},\boldsymbol{u})}{\partial \boldsymbol{x}} \end{bmatrix}^\intercal \boldsymbol{\lambda} + \frac{\partial p(\boldsymbol{g}(\boldsymbol{x},\boldsymbol{u}))}{\partial \boldsymbol{x}} = 0 \tag{3-67}$$

$$\frac{\partial L(\boldsymbol{x},\boldsymbol{u},\boldsymbol{\lambda})}{\partial \boldsymbol{u}} = \frac{\partial F}{\partial \boldsymbol{u}} + \begin{bmatrix} \frac{\partial \boldsymbol{W_P}(\boldsymbol{x},\boldsymbol{u})}{\partial \boldsymbol{u}} \\ \frac{\partial \boldsymbol{W_Q}(\boldsymbol{x},\boldsymbol{u})}{\partial \boldsymbol{u}} \end{bmatrix}^\intercal \boldsymbol{\lambda} + \frac{\partial p(\boldsymbol{g}(\boldsymbol{x},\boldsymbol{u}))}{\partial \boldsymbol{u}} = 0 \tag{3-68}$$

The above optimality conditions can be used to compute optimisation steps for the control variables by executing the following steps:

Step 1

The first optimality condition $\frac{\partial L(\boldsymbol{x},\boldsymbol{u},\boldsymbol{\lambda})}{\partial \boldsymbol{\lambda}} = 0$ represents the power flow equations. These power flow equations can be solved using Newton-Raphson's method or any other power flow method. In this case study, Newton-Raphson's power flow method as described in Section 3-1-1 is used. In the first iteration, the maximum power output value of the controllable generators can be used as initial starting point of the algorithm. However, if more educated initial values are available, these should be used. For example, if the OPF is solved for multiple time steps, the optimized control variables of the time step can be used as initial values for this optimisation.

Step 2

From the second optimality condition, an updated $\boldsymbol{\lambda}$ can be determined:

$$\boldsymbol{\lambda} = -\begin{bmatrix} \frac{\partial \boldsymbol{W_P}(\boldsymbol{x},\boldsymbol{u})}{\partial \boldsymbol{x}} \\ \frac{\partial \boldsymbol{W_Q}(\boldsymbol{x},\boldsymbol{u})}{\partial \boldsymbol{x}} \end{bmatrix}^{\intercal^{-1}} \left(\frac{\partial F}{\partial \boldsymbol{x}} + \frac{\partial p(\boldsymbol{g}(\boldsymbol{x},\boldsymbol{u}))}{\partial \boldsymbol{x}} \right) \tag{3-69}$$

Step 3

The objective function at any new point $\boldsymbol{u}^{(k+1)}$ can be approximately expressed using the second-order Taylor series expansion with respect to the known point $\boldsymbol{u}^{(k)}$:

$$L(\boldsymbol{x},\boldsymbol{u}^{(k+1)},\boldsymbol{\lambda}) \approx L(\boldsymbol{x},\boldsymbol{u}^{(k)},\boldsymbol{\lambda}) + \left[\frac{\partial L(\boldsymbol{x},\boldsymbol{u}^{(k)},\boldsymbol{\lambda})}{\partial \boldsymbol{u}} \right]^\intercal \boldsymbol{\Delta u} + \frac{1}{2} \boldsymbol{\Delta u}^\intercal H \left(\boldsymbol{x},\boldsymbol{u}^{(k)},\boldsymbol{\lambda} \right) \boldsymbol{\Delta u} \tag{3-70}$$

where H is the Hessian matrix of the second order partial derivatives of L with respect to $\boldsymbol{u}$. For the optimal $\boldsymbol{\Delta u}^*$, the gradient of this function to $\boldsymbol{\Delta u}$ equals 0. Therefore, this approximated optimal change in control variables can now be computed as follows:

$$\frac{\partial L(\boldsymbol{x},\boldsymbol{u}^{(k+1)},\boldsymbol{\lambda})}{\partial \boldsymbol{\Delta u}} \approx \frac{\partial L(\boldsymbol{x},\boldsymbol{u}^{(k)},\boldsymbol{\lambda})}{\partial \boldsymbol{u}} + H(\boldsymbol{x},\boldsymbol{u}^{(k)},\boldsymbol{\lambda}) \boldsymbol{\Delta u}^* = 0 \tag{3-71}$$

$$\boldsymbol{\Delta u}^* \approx -H \left(\boldsymbol{x},\boldsymbol{u}^{(k)},\boldsymbol{\lambda} \right)^{-1} \frac{\partial L(\boldsymbol{x},\boldsymbol{u}^{(k)},\boldsymbol{\lambda})}{\partial \boldsymbol{u}} \tag{3-72}$$

The term $\frac{\partial L(\boldsymbol{x},\boldsymbol{u}^{(k)},\boldsymbol{\lambda})}{\partial \boldsymbol{u}}$ can be directly determined from the third optimality condition (3-68). The Hessian H should be determined taking the partial derivative of (3-68) with respect to $\boldsymbol{u}$.

Step 4

The control variables can be updated using $\boldsymbol{\Delta u}^*$ from Step 3: $\boldsymbol{u}^{(k+1)} = \boldsymbol{u}^{(k)} + \beta \boldsymbol{\Delta u}^*$. Here, β is the step size, which is a positive value. This step size can be adjusted to improve the convergence rate of the algorithm. The values of $\boldsymbol{u}$ are restricted by the maximum and minimum power output of the controllable generators. Therefore, after updating the control variables $\boldsymbol{u}$, the values are clipped to the minimum and maximum values.

Step 5

Convergence of the algorithm is now checked using convergence criteria. Possible convergence criteria are:

- Change in objective function between current and previous iteration being less then prescribed tolerance value;
- Change in control values $\boldsymbol{\Delta u}$ being less than prescribed tolerance value.

In this case study, the change in objective function is chosen as the convergence criterion. If the algorithm has not converged yet, the algorithm is repeated from Step 1.

This Newton's algorithm based OPF method is used in the following contingency control method.

3-3 Differential evolution algorithm

Differential evolution is a specific type of evolutionary algorithm. An evolutionary algorithm is a stochastic search and optimisation algorithm which mimics natural evolution principles [50]. The main imitated principle is the survival of the fittest. In this, the three genetic operators of reproduction, mutation and crossover play an important role.

Preventive-corrective contingency control using DE is used by both [54] and [55]. The difference between both approaches is the parameter choice for the members of the population. This can be regarded as the search space of the algorithm. In [54], the members of the population are differentiated based on the maximum active power output of the controllable generators. In [55], binary parameters are used to describe whether a contingency will be solved in a preventive or a corrective manner. The required population size is directly proportional to the number of parameters of each population member. The size of the population is closely related to the computational complexity of the algorithm. Therefore, if the number of considered contingencies is larger than the number of controllable generators, which is true for this case study, the approach of [54] is favourable.

The working principle of the DE algorithm as described in [54] is visualised in Fig. 3-3. The following process steps are shown in the figure:

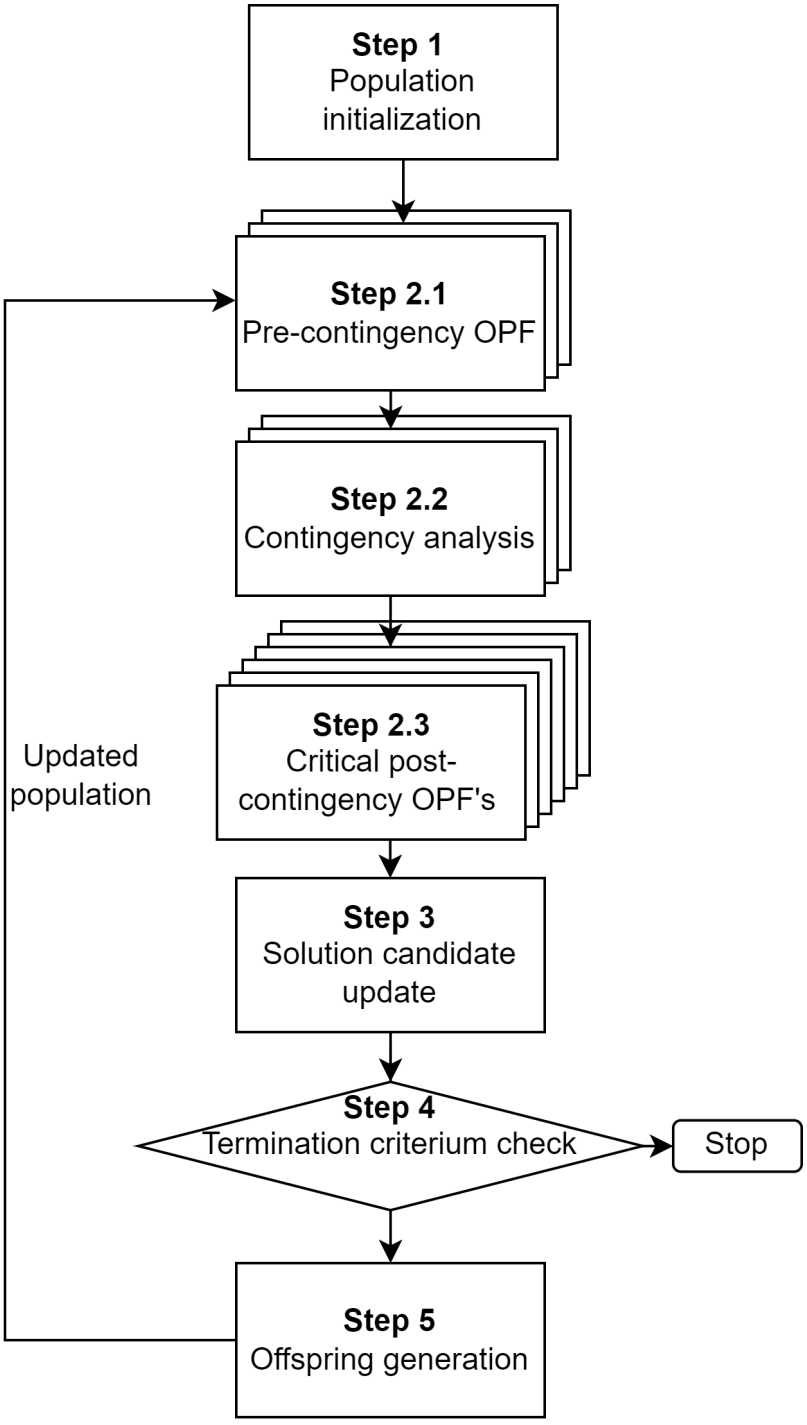

Figure 3-3: DE-based preventive-corrective control method, adepted from [54].

Step 1

An initial population is selected. Every member of this population has a unique set of parameters. The members consist of a set of maximum power output setpoints for the controllable distributed energy resources (DER) generators. The values represent fractions of the actual maximum power output and are therefore within the $[0, 1]$ interval. If there is no information on the position of the optimal setpoints, the initial population is selected randomly based on this $[0, 1]$ interval. However, if more information on the optimal setpoints is known, the initial population can be selected more specifically. For example, it might be known that the optimal setpoints for all generators are larger than 0.5, the initial population can be randomly selected in the interval $[0.5, 1]$.

Step 2

In this step, all the fitness of all members of the population is evaluated. In this case, the fitness of the members of the population is evaluated by means of two criteria:

- The costs of preventive control actions C_{pc}. These control costs are defined as $C_{pc} = \sum_{j \in S_{\mathrm{CG}}} c_j \left(P_{G,j}^{\max} - P_{G,j}\right)^2$, where S_{CG} is the set of controllable generators, c_j is a generator-specific control cost parameter, $P_{G,j}^{\max}$ is the original maximum power output of generator j and $P_{G,j}$ is the preventive control value for generator j. In [54], the corrective control costs are also included in the control costs. However, as the authors of [8] rightfully point out, this requires an accurate estimate of the failure probability of any grid component. Moreover, the main goal in pre-contingency state is to minimize power curtailment, thus preventive control actions. However, in emergency post-contingent situations, secure grid operation is of utmost importance and the costs of corrective control actions are not as important. Therefore, only the preventive control costs are included in the cost function.

- The number of contingencies for which the limit violations can not be mitigated in the required time frame after a contingency happened. Members with less of critical contingencies are always considered more fit than members with more of these, regardless of their C_{pc}. This ensures that the algorithm converges towards solutions with no critical contingencies.

To define the preventive control costs and critical contingencies for each member of the population, three substeps are taken. First of all, the pre-contingency OPF is solved, given the maximum power output setpoints of all controllable generators, defined for each member. Then, contingency analysis is performed for these setpoints, to analyse which contingencies require additional corrective control actions. If the loading of a grid component exceeds 150% immediately after a contingency occurred, given the particular preventive control actions, this contingency is marked as a critical contingency, for which no corrective control action can compensate. In current Stedin safety practice, components will shut off when the detected loading exceeds 150%, because of the potential damage to the grid component. Finally, a post-contingency OPF is solved for each of the contingencies which require additional corrective control actions. If no possible control actions mitigate the constraint violations within the selected time frame, these contingencies are also labelled as critical contingencies.

Using the set of critical contingencies and the preventive control setpoints, the fitness of each member of the population is evaluated.

Step 3

In the third step, the solution candidate is updated. To do this, the selection procedure is executed first. Every members of the current population is compared to a member of the previous population. The member with the smallest number of critical contingencies is selected and will be a parent member for the next iteration. If both members share the same number of critical contingencies, the member with the smallest C_{pc} is selected.

Out of all the selected parent members, the member with no critical contingencies and smallest C_{pc} is selected as solution candidate. If there are no members without critical contingencies, the member with smallest number of critical contingencies is selected. If multiple members share this number of contingencies, the member with smallest cost is selected.

Step 4

The convergence criteria of the DE algorithm are now checked. Possible convergence criteria are: (i) best member of current population is not better than best member of previous iteration for a predetermined number of iterations or (ii) maximum number of iterations is reached. If the convergence criteria are not met, the iterations continue. It is worth to mention that it is advised against to use criteria (i) for only one iteration. Especially with relatively small population size, the probability that the best member of the current population is not better than the best member of the previous population is significant. It is shown in [13] that the best candidate might not improve for multiple iterations, although it has not yet converged to the optimum. Since the maximum number of non-improving iterations while not converged can not be determined, a maximum total number of iterations is used as stopping criteria in this study.

Step 5

Now, a new population is generated, based on mutation and crossover operators. The objective of mutation is to diversify the parameter space of the members of the population, while at the same time steer the population members to the optimal values within reasonable time period. In DE, new population members are generated by adding the scaled difference of two parent members to a third member. So:

$$x_i' = x_i + F(x_{r_1} - x_{r_2}) \tag{3-73}$$

where x_i' is the new member, x_{r_1} and x_{r_2} are randomly selected old population members and F is a scaling factor in the range $\langle 0, 1]$. Furthermore, $r_1 \neq r_2 \neq i$, since x_i' should be a mutation, and not just a linear combination of two members. An optional addition to this operation is a scaled version of the difference between the base vector x_{r_3} and the current solution candidate, thus:

$$x_i' = x_i + \lambda(x_{\text{best}} - x_i) + F(x_{r_1} - x_{r_2}) \tag{3-74}$$

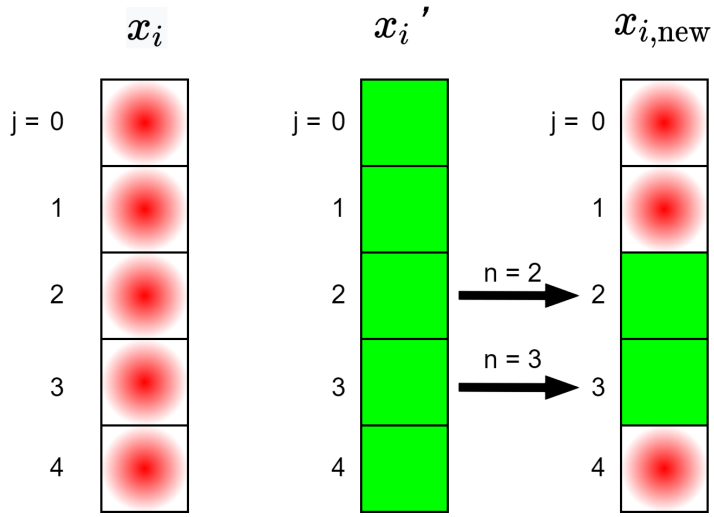

Figure 3-4: Visuzaliation of crossover operator for $D = 5$, $n = 2$ and $L = 3$, adepted from [41]

where λ is a scaling factor in the range $\langle 0, 1]$, but generally significantly smaller than F, to avert premature convergence.

The second important operator in the generation of a new population is crossover. This operator aims to increase the diversity of parameter vector. After the mutation operator, the crossover operator selects certain values of the newly mutated members to replace values of the old member at that index. There are various ways to select the parameters to crossover. In [41], where DE is introduced, crossover is performed in the following manner:

$$(x_{i,\text{new}})_j = \begin{cases} (x'_i)_j & \text{for} \quad j = \langle n \rangle_D, \langle n+1 \rangle_D, \ldots, \langle n+L-1 \rangle_D \\ (x_i)_j & \text{for all other} \quad j \in [0, D-1] \end{cases} \tag{3-75}$$

where the brackets $\langle \rangle_D$ denote the modulo function with modulus D and D is the number of parameters of each member, thus in this case the number of controllable generators. So if the value inside the brackets is larger than D, the remainder of the division of the value over D is returned. In (3-76), n is a randomly chosen integer from the interval $[0, D-1]$. Integer L denotes the number of parameters to be selected and is drawn from the interval $[1, D]$. This crossover operation is visualised in Fig. 3-4.

In [50], a different crossover operation is proposed. Instead of subsequent crossover variables, the probability of crossover is set for each variable of each member of the population. This means that there is no cross-correlation between crossover probability of two separate variables. The same authors also propose another alternative to this discrete crossover operator. Instead of a crossover probability, leading to a discrete crossover, a continuous crossover is proposed as follows:

$$x_{i,\text{new}} = x_i + f_2(x_{r_3} - x_i) + F(x_{r_1} - x_{r_2}) \tag{3-76}$$

It can be observed that if $f_2 = 1$, the model represents a discrete crossover and mutation model with a crossover probability equal to 1. If $f_2 = 0$, the model reduces to the mutation-only model of (3-74). In [50], it is mentioned that with a population size of $20D$, $F = 0.8$ and $f_2 = 0.5$ appear to be good values for the DE process. It is also stated that the population size

can range between $2D$ and $100D$. In [54], a population size of $6D$ is proposed. Different DE models as described above with different tuning parameter values will be used and analysed in the case study.

Now, using the new population, the algorithm is repeated, starting from Step 2.

3-4 Results of differential evolution-based contingency control method

In this section, the results of the DE-based contingency control method on the case study as presented in Chapter 2 will be discussed. For the performance of the algorithm, a few design choices are relevant. First of all, the specific DE model should be chosen. For this case study, the discrete crossover and mutation model as used in [50] is used. The number of controllable generators in the case study is only 4, and therefore the crossover operator of [41] as visualised by Fig. 3-4 is not expected to add significant value, compared to the discrete crossover model. Furthermore, the continuous crossover and mutation model of (3-76) is used, since this continuous model might have an influence on the performance of the algorithm. For this continuous model, different F and f_2 parameter settings will be compared. Furthermore, the population size is generally considered to have an important impact. If the population size is too small, the convergence over subsequent iterations will be slow and the risk of premature convergence will be large. However, increasing the population size increases the computational time to compute each iteration.

The contingency control method is evaluated for different moments in time. The results for two moments in time are shown in this section. For results on more moments in time, Appendix A can be consulted.

3-4-1 Crossover and mutation model design

To select the appropriate crossover and mutation model, different model designs are investigated as mentioned above. The continuous crossover and mutation model is evaluated for scaling factors $F = 0.8$ and $f_2 = 0.5$, as suggested by [50] and $F = 0.6$ and $f_2 = 0.35$. Furthermore, the discrete crossover and mutation model will be evaluated for the crossover probability $p_{CR} = 0.85$ and probability $p_{CR} = 0.95$. These are both within the range of 0.8 to 1, suggested by the authors of [50].

Since the first and foremost goal of the contingency control method is to mitigate the potential risks of critical contingencies, one could expect an analysis of the capability of the controller design to mitigate critical contingencies. However, since the members with less critical contingencies are always considered more fit than the members with more critical contingencies, the DE algorithm easily converges to a solution with no critical contingencies. The main challenge of the algorithm is to converge to a solution with minimal preventive control costs C_{pc}. Therefore, the evolution of the C_{pc} of the best population member is analysed to select an appropriate crossover and mutation model design.

In Fig. 3-5, the evolution of the C_{pc} is presented for July 1^{st} at noon for different DE model designs and different population sizes. The same results are shown for July 6^{th} in Fig. 3-6. In these figures, D is again the number of controllable generators.

From these figures, it can be observed that there is no clear superior crossover and mutation model. It can be concluded from this data that the different design choices in this model do not influence the convergence rate significantly. The tested model designs are all within the derived preferable boundaries of previous studies [50,54], which explains why the performance of these different models does not diverge significantly. With increasing population size, the difference of results between the different models further diminishes. This was to be expected, since in a larger population, the crossover and mutation operators are applied to a population member relatively less frequently, compared to a smaller population. The influence of different operator options therefore diminishes.

Given the above observations, the continuous model with $F = 0.8$ and $f_2 = 0.5$ is selected for this case study. Now, the population size design choice for this model is discussed.

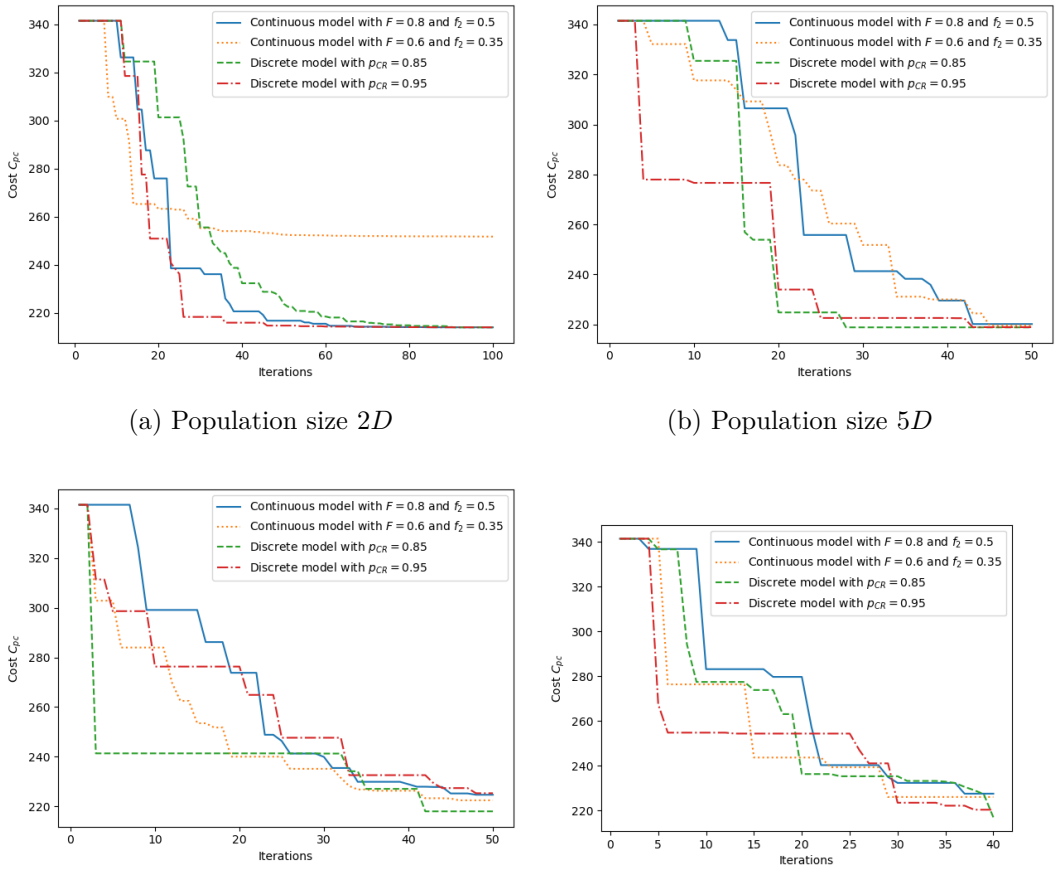

(a) Population size $2D$

(b) Population size $5D$

(c) Population size $10D$

(d) Population size $20D$

Figure 3-5: Preventive control cost evolution for different model designs on July 1st, given different population sizes.

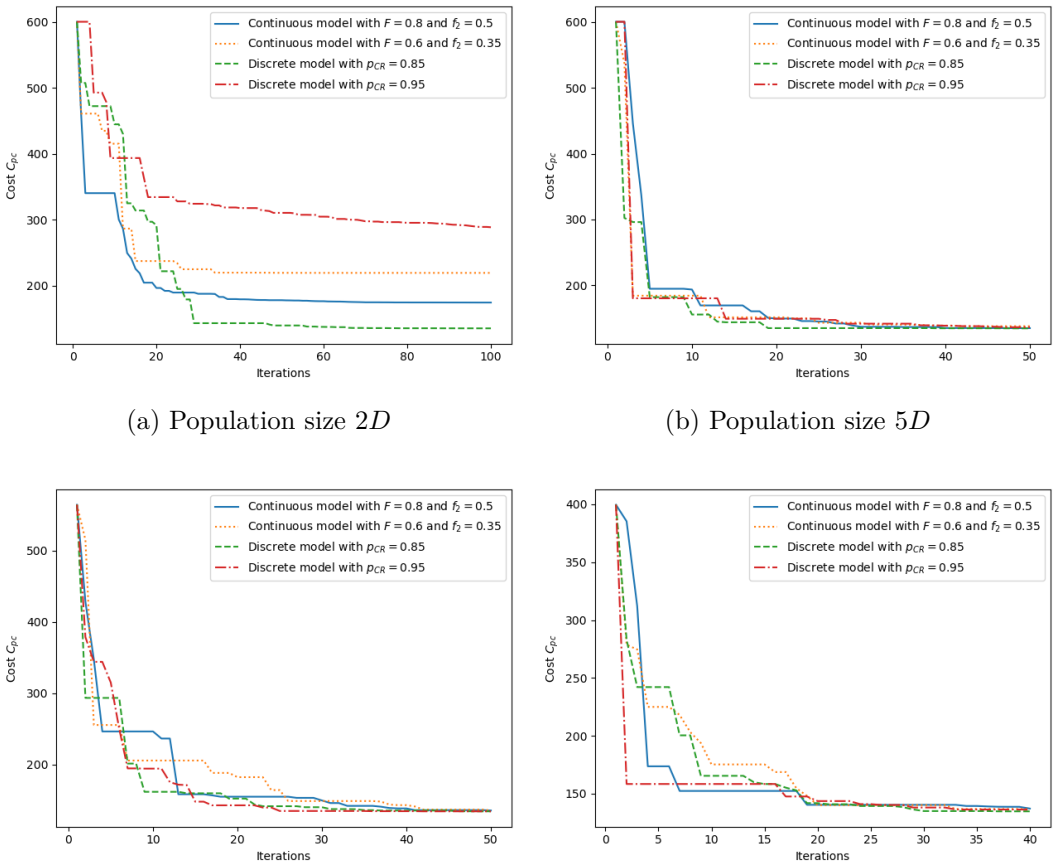

(a) Population size $2D$

(b) Population size $5D$

(c) Population size $10D$

(d) Population size $20D$

Figure 3-6: Preventive control cost evolution for different model designs on July 6$^{\text{th}}$, given different population sizes.

3-4-2 Population size

Now that the crossover and mutation model has been evaluated, an analysis on the population size remains. The population size has major influence on the risk of premature convergence, the convergence rate and computational complexity of the DE algorithm. First of foremost, premature convergence should be prevented, since this diminishes the performance of the algorithm. Then, an analysis has to made between the computational complexity of an iteration and the convergence rate per iteration. To this end, the C_{pc} will be evaluated over time, instead of over iteration. The results of the evolution of C_{pc} over time using different population sizes is shown in Fig. 3-7 for July 1$^{\text{st}}$ and Fig. 3-8 for July 6$^{\text{th}}$.

Note that the evolution lines do not share the same starting time. The first data point is the cost after one iteration. The time it takes to perform this first iteration is not equal for all population size. From the figures, it can be observed that the population size $20D$ is too large. Due to the time it takes to perform one iteration, the time to converge is large. The same holds to a lesser extent for population size $20D$. The population size $2D$ on the other hand requires a lot of iterations and in many cases does not improve for a large

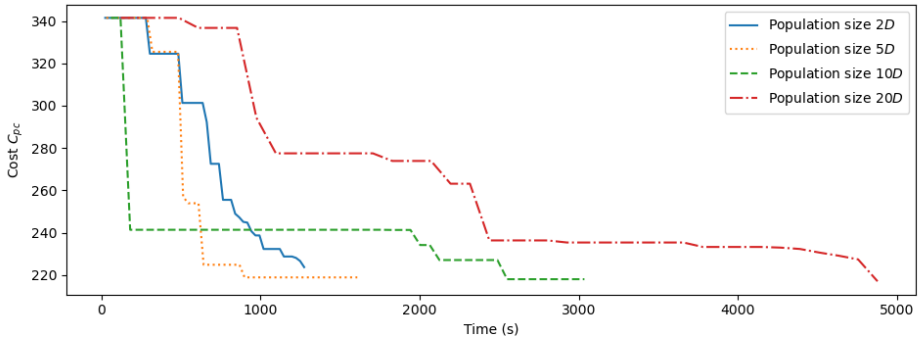

Figure 3-7: Preventive control cost evolution for different population sizes on July 1st.

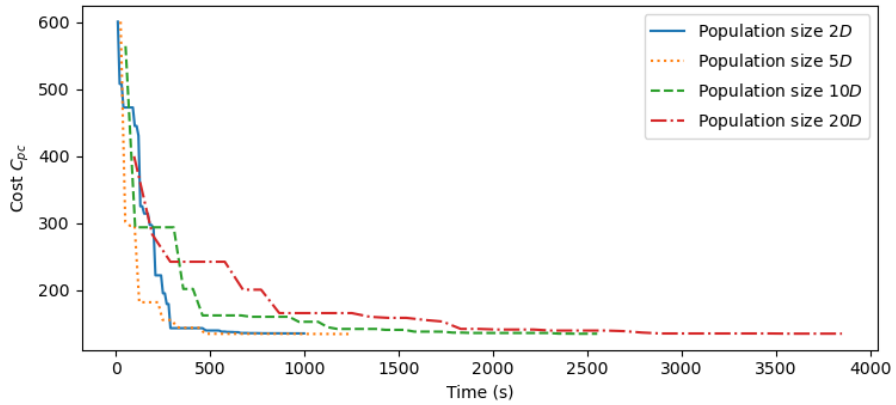

Figure 3-8: Preventive control cost evolution for different population sizes on July 6th.

number of iterations. This makes it hard to define the convergence criterion based on the improvement of the best population member. Moreover, in Fig. 3-5 and Fig. 3-6, it can be observed that the population size $2D$ frequently leads to premature convergence. For this reason, the population size of $5D$ seems to be adequate for this contingency control problem on this case study. This coincides with the findings of [54], where a population size of $6D$ is used. In [13], a maximum number of iterations of 30 is used, which does not suffice for all scenarios in this case study. Therefore, the number of iterations is set to 40. After 40 iterations, the evolutionary algorithm is converged in all tested scenarios.

3-4-3 Visualisation of preventive-corrective contingency control

Now that the parameters of the contingency control design are defined, the working principle of this control method can be visualised. The visualisation is based on the loading limits of the grid components. In Fig. 3-9 and Fig. 3-10, the power output of the controllable DER connections and the loading of grid components is shown for different situations: the pre-contingent situation, the post-contingent situation directly after contingency occurrence, when no corrective control actions are applied yet, and the post-contingent situation after 30 seconds, when the optimal corrective control actions are applied. In Fig. 3-9, this is shown for corrective control, where the power output of the controllable DER is not restricted in a

preventive manner. It can be observed that the corrective control actions after the contingency occurred are not capable to mitigate the loading violations in time, because of the constraint on the curtailment ramp of the connections. In Fig. 3-10, it can be observed that the power output of the controllable DER connections is already curtailed in a preventive matter, to make sure that the allowed corrective control actions are sufficient to mitigate the loading violations in time. The loading of the critical component after preventive-corrective control actions is 100.23%, which means it is still slightly overloaded. This 0.23% is due to the minor inaccuracy of the OPF algorithm. This error is considered to be acceptable as long as the loading is smaller than 101%. This overloading would likely not lead to any serious damage to the components and can be resolved quickly.

3-4-4 Extra grid capacity due to contingency control

The DE-based contingency control algorithm is performed on 1972 randomly selected daytime timepoints in one year. Given the preventive-corrective power output setpoints of this dataset, the total share of active power curtailment due to preventive control actions can be determined. On the other hand, it would be interesting to determine the extra renewable energy power generation that preventive-corrective control would allow on a power grid, compared to a situation in which only restricted corrective actions could have been applied. To determine this, the for each generator, the maximum curtailment percentage of a generator during all timepoints is used to scale that generator down. This means that the generator is dimensioned to prevent any preventive actions to be necessary at all. In Table 3-3, the results for the situation where no control is applied, the preventive-corrective control situation and the scaled generator situation with only corrective control are shown.

	Gen. 1	Gen. 2	Gen. 3	Gen. 4
No Control	100%	100%	100%	100%
Preventive-corrective control	99.6%	98.7%	97.89%	94.1%
Scaled generator situation	88.6%	39.1%	66.9%	8.5%

Table 3-3: Percentage of DER energy share for different scenarios

It can be observed that the scaling the generators to the worst moment in time reduces the amount of renewable energy share tremendously. However, using a preventive-corrective control algorithm, only up to 6% of the energy output is curtailed in a preventive way. In the case of no control, 100% of all possible renewable energy is delivered to the power grid. However, this would lead to potentially insecure grid situations in case of critical contingencies.

3-4-5 Computational complexity

The computational time of the DE iteration for the Middelharnis power grid considered in this study ranges from 351 to 2481 seconds and the average time is 970 seconds. The required time hugely depends on the number of optimal power flows and contingency analyses to be executed. These numbers differ between scenarios. The average number of executions per scenario and the average computation time per execution is shown in Table 3-4. The percentage of computation time used by these different processes compared to the total computation

time is also presented in the same table. Reducing the time to compute the optimal power flow and to perform contingency analysis would be effective measures to decrease the total computational complexity of this contingency control method.

The computational complexity of the OPF in this case study is high compared to data from literature. For example, in [13], the OPF for a slightly smaller system takes 0.05 seconds to compute. In that research, the MATPOWER package is used to compute the OPF, which uses advanced solvers, mainly based on the interior point method. Using different methods to solve the OPF is not further researched in this thesis, but is recommended in further research efforts.

	OPF	Contingency analysis	Other operations
Average number of executions (-)	2360	800	-
Average computational time per execution (s)	0.32	0.36	-
Percentage of computation time	70%	27%	3%

Table 3-4: Computational effort of different contingency control process operations

3-5 Conclusions

The preventive-corrective contingency control based on differential evolution is able to define suitable preventive and corrective control measures for the case study of this thesis. From the traditional contingency analysis methods, the full AC power flow method is the preferable method, due to its accuracy and the limited computational benefit of the LODF-based method.

The crossover and mutation model design is based on the performance results of different parameter settings. The continuous model with $F = 0.8$ and $f_2 = 0.5$ was selected as favourable design option. However, other designs within the ranges previously determined by other academic efforts could also be selected. The most critical parameters are the population size and maximum number of iterations, which are set to $5D$ and 40, respectively, where D is the number of considered contingencies.

The resulting preventive-corrective contingency control method is capable to keep the power grid in secure state, while only reducing curtailing up to 6% of the active power, for this case study. An alternative where all preventive control actions are avoided by dimensioning the DER connections to the worst case moment in time delivers far worse performance in terms of renewable energy share.

The control method is computationally too complex to deliver realtime preventive and corrective control actions, since the algorithm takes on average 970 seconds to converge. The power flow on the distribution grid has a dynamic nature, especially when the DER penetration is high. Therefore, efforts should be made to decrease the computational complexity of this control method.

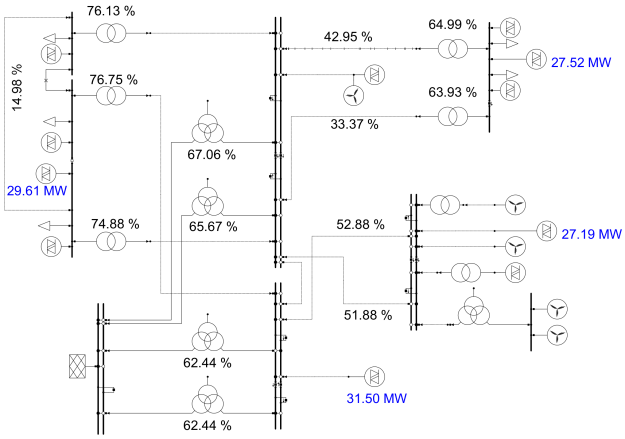

(a) Pre-contingent situation with no control actions applied

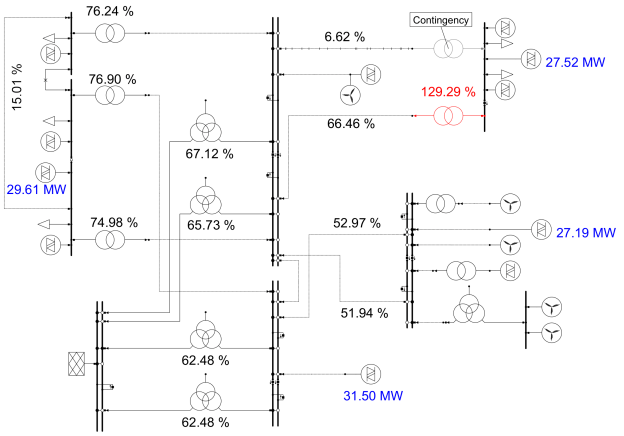

(b) Post-contingent situation with no control actions applied

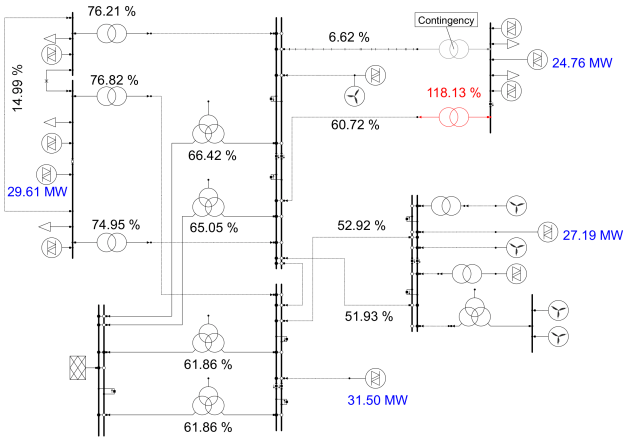

(c) Post-contingent situation with corrective control actions applied

Figure 3-9: Corrective contingency control example

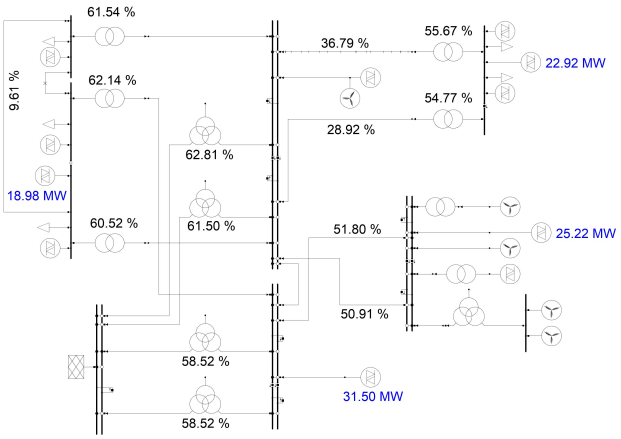

(a) Pre-contingent situation with preventive action applied

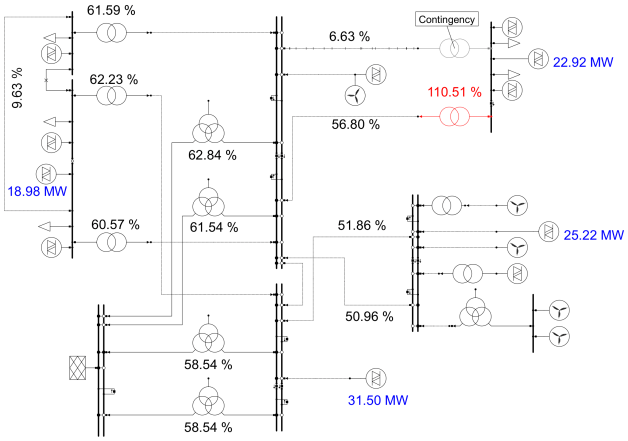

(b) Post-contingent situation with only preventive action applied

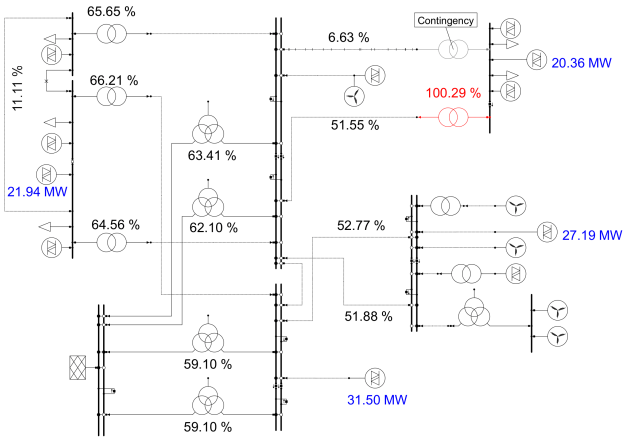

(c) Post-contingent situation with corrective control applied

Figure 3-10: Preventive-corrective contingency control example

Chapter 4

Use of convolutional neural networks in preventive-corrective control

Because of the dynamic nature of the load and generation on a distribution grid, especially considering volatile distributed energy resources (DER), the computational times of the contingency control method based on differential evolution (DE) as presented in Chapter 3 can generally be considered not sufficient to guarantee secure grid operation, because of the delay between the power grid situation and adequate control actions.

Machine learning has proven to be a useful study to reduce online computational complexity for a wide variety of optimisation problems in power grid operation. There are multiple studies where machine learning is used to define corrective control actions as in [5, 11, 22, 58]. The authors of [11,22] and [5] describe local, decentralized machine learning methods to determine local control variables. This could be mainly interesting for large scale distribution grids, where realtime data collection and communication is an issue. In [58], Q-learning is used to perform contingency control. The authors of this method stress the challenges of this method on convergence and reasonable learning time, optimality of the policy and scalability. Besides, training this algorithm would require either dynamic simulation or physical implementation, which adds to the problem of reasonable learning time. The studies all show that machine learning techniques are capable to compute adequate control actions in a short time frame.

There are also very promising results in the use of machine learning for contingency analysis [13, 17, 44, 52, 53, 56], which is a computationally intensive step in the process of contingency control, as is discussed in Section 3-4. In [44] and [17], artificial neural networks are used to determine the influence of a contingency on the grid situation. In [53], neural networks are combined with concentric relaxation. This concentric relaxation exploits the attribute that the critical influence of a contingent component is usually limited to the grid components nearby [51]. Therefore, the method in [53] might be specifically interesting for larger distribution power grids. In [13], a convolutional neural network (CNN) is used to this end. Convolutional neural networks are an extension on neural networks and are capable to detect patterns in input samples. These networks are commonly used in image classification, because the visual

patterns in images form a suitable basis for classification. The results in [13] show improved results compared to methods without convolutional layers.

To the author's knowledge, there are no efforts in literature where machine learning techniques increase the computational efficiency of preventive-corrective control problems. The promising results for corrective control and contingency analysis, combined with the need for improved computational efficiency in preventive-corrective control, calls for an effort on the application of machine learning techniques for preventive-corrective control. Based on the analysis above, the CNN is the most promising technique for preventive-corrective control. This is a centralized method which has proven improved performance compared to standard neural network approaches and it is suitable for different sized distribution power grids.

In this chapter, neural network techniques will be applied to contingency analysis and contingency control processes. First, the CNN is introduced in Section 4-1. Then, using CNN to perform contingency analysis as a process step of preventive-corrective control is discussed in Section 4-2. Furthermore, the use of neural networks, for the complete process of contingency control is presented in Section 4-3. Conclusions on these methods are drawn in Section 4-4.

4-1 Convolutional neural networks

Artificial neural networks are developed to mimic biological neural networks used by humans and animals to process complex tasks efficiently. These artificial neural networks are frequently applied in engineering to perform nonlinear approximation and classification. This is done by passing an input through different layers of neurons, which all apply a weight to the input, before passing it through to the next neuron. The weights on the inputs are updated based on known input and output data, which is called the learning process. Furthermore, activation functions can be applied on layers of neurons. These nonlinear functions enable the network to learn nonlinear processes. Convolutional neural networks are an extension on neural networks. Instead of relatively simple multiplicative operations, convolution operations are performed in the convolutional layers. The convolution is defined as the integral of the product of the two functions after one is reversed and shifted and can be described for one-dimensional cases as:

$$(f * g)(t) = \int_{-\infty}^{\infty} f(\tau)g(t-\tau)d\tau \tag{4-1}$$

This convolution produces a function that expresses how the shape of function f is modified by function g for different shifts t. This operation can be used to extract features of inputs, using different filter functions, frequently named kernels. For the two-dimensional case, the operation is as follows [13]:

$$O(i,j) = \sum_{u=0}^{c-1}\sum_{v=0}^{c-1} I(i+u, j+v) \cdot H(u,v) + b \tag{4-2}$$

where O is the output feature map for filter H on input data I. Parameter c represents the size of the filter and b is the bias parameter. This operation is visualised for one filter H for the two-dimensional case in Fig. 4-1. The output is constructed by shifting all filters over the input. This output is called a feature map, since it contains the different features

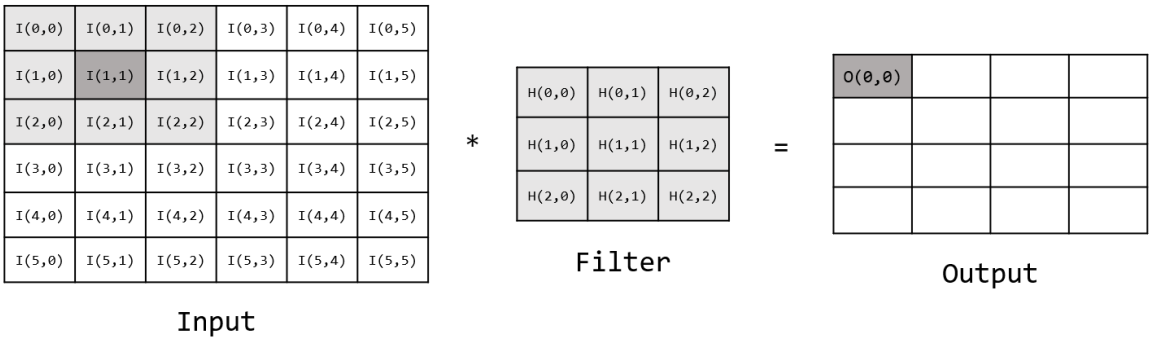

Figure 4-1: Schematic of convolutional operation of neural network, adepted from [4]

in different parts of the input. Multiple sequential convolutional layers can be used. The feature map from the previous layer is used to extract other, more complex, features in the next layer. The use of convolutional layers in neural networks is introduced in [26], where this method is used to recognize handwritten zip codes on postal items. The convolutional neural network approach relies on sparse connectivity of the input. This means that the output of the network is largely dependent on the relation of an input data point with its nearby data points. Therefore, the method is frequently used for image classification. However data with a grid-like topology, such as power network data, is also sparsely connected, since the influence of buses on nearby buses is relatively large.

In this research, all neural networks are learned using the Adam optimisation method originating from [23], which is a first order stochastic gradient optimisation algorithm.

4-2 Use of convolutional neural network in contingency analysis

As mentioned before, a deep convolutional neural network is used to perform contingency analysis in [13]. It is shown that this CNN-based approach is very fast compared to the model-based approach and significantly more accurate than the artificial neural network approach. Furthermore, we have shown in Section 3-4-5 that 27% of the computational time of the preventive-corrective control algorithm is directly attributed to the contingency analysis operation. Therefore, the CNN-based method to perform contingency analysis is implemented in this section.

4-2-1 Neural network design

The design of the neural network is displayed in Fig. 4-2. As can be observed from Fig. 4-1, the convolutional layer reduces the dimensions of the data, due to the size of the filters. To maintain the input dimensions in the convolutional layer, cell padding is applied. This technique augments the input data such that the output dimension matches the original input dimension. Furthermore, as the final activation function for Output 2, classifying the security state, the Softmax activation function is used, which is described by:

$$\sigma_i(\mathbf{z}) = \frac{e^{z_i}}{\sum_{j=1}^{K} e^{z_j}} \tag{4-3}$$

where **z** is the input vector. This function ensures that all output values of the function will sum to 1. These final values can be considered as the probability that the system is in the corresponding security state.

4-2-2 System security state definition and loss function

The neural network is aimed to identify three different security states: safe, alarm and insecure. In safe security state, there is no threat of overloading grid components or voltage violations. In alarm security state, the system is close to insecure security state, so components might be almost overloading or voltage violations almost occur. In insecure security state, components are overloaded and/or voltage violations exist. This security state is based on a security index I_S. The security index as presented in [44] is used in this research:

$$I_S = \left[\sum_i \left(\frac{d_{v,i}^{(u)}}{g_{v,i}^{(u)}} \right)^4 + \sum_i \left(\frac{d_{v,i}^{(l)}}{g_{v,i}^{(l)}} \right)^4 + \sum_l \left(\frac{d_{p,l}}{g_{p,l}} \right)^4 \right]^{1/4} \tag{4-4}$$

where

$$d_{V,i}^{(u)} = \begin{cases} \frac{V_i - F_i^{(u)}}{V_{i,\text{nom}}} & \text{if} \quad V_i > F_i^{(u)} \\ 0 & \text{if} \quad V_i \leq F_i^{(u)} \end{cases} \tag{4-5}$$

$$g_{V,i}^{(u)} = \frac{V_i^{(u)} - F_i^{(u)}}{V_{i,\text{nom}}} \tag{4-6}$$

$$d_{V,i}^{(l)} = \begin{cases} \frac{F_i^{(l)} - V_i}{V_{i,\text{nom}}} & \text{if} \quad V_i < F_i^{(l)} \\ 0 & \text{if} \quad V_i \geq F_i^{(l)} \end{cases} \tag{4-7}$$

$$g_{V,i}^{(l)} = \frac{F_i^{(l)} - V_i^{(l)}}{V_{i,\text{nom}}} \tag{4-8}$$

$$d_{L,j} = \begin{cases} \frac{L_j - L_{F,j}}{100\%} & \text{if} \quad L_j > L_{F,j} \\ 0 & \text{if} \quad L_j \leq L_{F,j} \end{cases} \tag{4-9}$$

$$g_{L,j} = \frac{L_{P,j} - L_{F,j}}{100\%} \tag{4-10}$$

In these equations, the following variables are defined:

V_i: the voltage level at bus i
$F_i^{(u)}$: the upper voltage alarm limit for bus i
$V_i^{(u)}$: the upper voltage security limit for bus i
$V_{i,\text{nom}}$: the nominal voltage at bus i
$F_i^{(l)}$: the lower voltage alarm limit for bus i
$V_i^{(l)}$: the lower voltage security limit for bus i
L_j: loading percentage of grid component j
$L_{F,j}$ alarm loading limit of grid component j
$L_{P,j}$ security loading limit of grid component j.

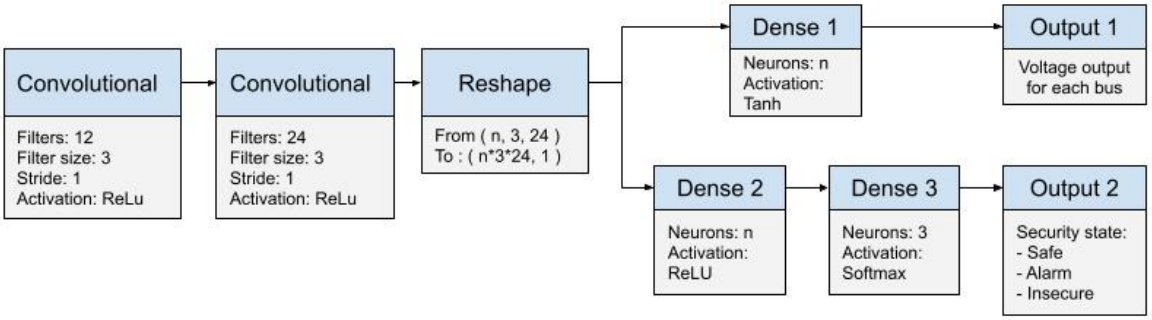

Figure 4-2: Convolutional neural network designed, based on [13]

Now, if $I_S = 0$, the system is in a safe state. If $0 < I_S \leq 1$, the system is in an alarm state. If $I_S > 1$, the system is in an insecure state. Using this index, contingencies can be ranked based on their severity. For the purpose of this CNN, the ranking is reduced the security state classification as described above to define Output 2. This means that the system is either classified as safe, alarm, or insecure. The categorical cross-entropy loss function is used for Output 2, since this is the most widely used loss function for multi-classification outputs [13].

For Output 1, the mean square error is used. This mean square error function is frequently used for continuous outputs. In contrast to the design in [13], a tanh activation function is used in the layer Dense 1. This activation layer allows a non-linear relationship between the feature map output of the convolutional layers and Output 1. Output 2, the security state output, it of foremost interest, since it is the main purpose of contingency analysis. It is therefore interesting to research whether a neural network with only Output 2 as output, could outperform the neural network as presented in Fig. 4-2. However, the voltage output data might be useful in the contingency control, for example to use as initial conditions for the optimisation problem. Therefore, two networks will be analysed: a network with only the system security state as output and a network with both the system security state and the voltage data as outputs.

4-2-3 Results

To train the convolutional neural network, the hourly data of one year of grid operation is used. This means that there are 8760 data samples for each analysed contingency. This data is split into training, validation and test data. The split between these different dataset is 80%, 10% and 10%, respectively. Training data is used to train the neural network and is fed into the learning process each epoch. The validation data is used to validate the trained network after the learning process. The main purpose of this data set is to detect and prevent overfitting. Hyperparameters, such as the number of epochs, layers and filters or neurons per layer can be determined using the validation data. The test data is only used in the final stage of the development of the neural network. The data is used to analyse the results of the network.

Inclusion of voltage angle and magnitude outputs

As stated in Section 4-2-2, two convolutional neural networks are investigated. The first network includes both outputs, the voltage and security state output, and the second network includes only the security state as an output. The results for the network including both outputs are shown in Table 4-1, while Table 4-2 presents the results when including only the security state output.

Grid	Epochs	Errors		Accuracy (%)	Unidentified insecure cases (%)	Training time (s)	Evaluation time (s)
		Voltage (p.u.)	Phase (deg)				
IEEE 9-bus	10	0.24	8.72	86.85	24.29	156	0.065
	50	7e-2	2.88	94.32	4.45	568	
	100	2e-2	2.82	97.04	0.84	1270	
CIGRÉ MV	10	1e-2	0.74	98.92	5.87	499	0.070
	50	5e-3	0.25	99.56	0.14	2442	
	100	6e-3	0.25	99.70	1.49	4305	
Middelharnis	10	1.4	30.9	80.69	48.78	1004	0.069
	50	3e-3	0.86	93.74	16.12	4945	
	100	3e-3	0.69	95.11	5.5	9244	
IEEE 39-bus	10	5e-3	2.42	92.42	12.75	6664	0.104
	50	6e-3	1.64	93.6	4.44	33078	
	100	3e-2	1.25	94.52	3.76	55560	

Table 4-1: Convolutional neural network results with both outputs

Grid	Epochs	Accuracy (%)	Unidentified insecure cases (%)	Training time (s)	Evaluation time (s)
IEEE 9-bus	10	87.99	21.7	75	0.065
	50	94.39	5.99	402	
	100	96.79	1.75	765	
CIGRÉ MV	10	99.42	1.56	282	0.070
	50	99.07	0	1438	
	100	99.66	1.44	2843	
Middelharnis	10	85.04	0.28	91	0.068
	50	92.89	4.39	443	
	100	93.63	0.84	883	
IEEE 39-bus	10	86.56	13.89	3031	0.102
	50	94.40	2.96	15187	
	100	93.64	3.14	28883	

Table 4-2: Convolutional neural network results with only security output

In these tables, the evaluation time is defined as the time it takes to evaluate the security state of the network for all considered contingencies, consisting of all lines and transformers. It can be observed that high classification accuracy is achieved for both neural network designs for all grids. Furthermore, the percentage of insecure cases which is classified as alarm or safe cases is low. The network design with only one output has comparable accuracy results compared to the network design using both outputs, while the training time is reduced by more than 50%. However, the evaluation time is not significantly influenced. This means that the voltage output comes at the cost of increased training time, without major increase in accuracy and evaluation time. The neural network design with two outputs should therefore only be used when the voltage output can be used at a later stage of the control process, for example as initial values for an optimisation step. In this case of this study, these initial values are actually used, so the CNN with two outputs is preferred.

Accuracy of convolutional neural network in contingency analysis

Table 4-1 shows that the classification accuracy of the CNN is higher than 94% for all power grids of this case study. Besides, the percentage of unidentified insecure cases is not larger than 5% over all different power grids. It can be observed that the percentage of unidentified insecure contingencies does not necessarily coincide with the overall accuracy of the network. The network is designed to classify all contingencies in three categories and the resulting network might not be equivalently accurate for all types of contingencies. Possible explanations for this could be overfitting on training data, non-representative data set in general or specific neural net design in which not all dynamics of the non-linear process can be learned. Since separate training, validation and test data is used, as is described in Section 2-2, overfitting is monitored and is not present. A non-representative data set is more reasonably, since the data set is limited. To reduce the likelihood of insecure contingency cases not to be considered in the following contingency control process, all alarm state cases could also be considered by default. However, this might increase the computational complexity of the contingency control algorithm, since the amount of considered contingencies is increased. This trade-off should therefore be considered with caution.

Comparison of full AC load flow, LODF-based and CNN-based method

The accuracy of the CNN-based method is significantly better than the method based on line outage distribution factor (LODF), as is clearly demonstrated in Table 4-3. Both in the overall accuracy as in the percentage of unidentified insecure contingencies, the CNN method is superior.

The comparison of computational times to perform contingency analysis is given in Table 4-4. It can be observed that the CNN method shows superior performance with respect to computational efficiency. For the smallest IEEE 9-bus grid, the CNN-based method is the slowest. For this power grid, the full AC power flow method is preferable, due to its accuracy and computational complexity. For the larger test grids, the CNN-based method is 3-17 times faster than the full AC power flow method. Compared to the LODF-based method, the CNN method is considerable faster for the IEEE 39-bus power grid, but slightly slower for the Middelharnis and CIGRÉ MV power grids. Further analysis of the evaluation time

Grid	LODF method		CNN method	
	Accuracy (%)	Unidentified insecure (%)	Accuracy	Unidentified insecure (%)
IEEE 9-bus	66.78	100	97.04	0.84
Middelharnis	90.34	6.32	95.11	5.5
CIGRÉ MV	97.95	9.78	99.70	1.49
IEEE 39-bus	90.39	23.62	94.52	3.76

Table 4-3: Accuracy-based comparison of LODF and CNN (both outputs) contingency analysis methods

results in Table 4-4 shows that the computational benefit of the CNN- and LODF-based methods compared to the full AC power flow method deteriorates when the number of buses and contingencies increases. For the CNN-based method, this is also found by the authors of [13]. This observation reduces the value of these alternative methods, since these methods would mainly be useful in large power grids, where the computational efficiency of the full AC power flow method is insufficient.

Grid	Evaluation time (s)		
	Full AC power flow	LODF	CNN
IEEE 9-bus	0.059	0.031	0.065
Middelharnis	0.33	0.052	0.069
CIGRÉ MV	0.22	0.052	0.070
IEEE 39-bus	1.80	0.179	0.104

Table 4-4: Comparison of evaluation time for all contingency analysis methods.

Given the accuracy and computational efficiency results, the CNN method is preferable for larger power grids if the computational complexity of the full AC load flow method is undesired, due to its accuracy compared to the LODF-based method. In situations where the accuracy is of minor importance, one could opt to use the LODF-based method for medium-sized power grids. It should be noted that the traditional full AC power flow and LODF methods excel in simplicity and their easy to implement nature. There is no need to perform any learning process and it is uncomplicated to adjust the method to an adjusted grid topology. The method is also more robust to previously unseen load and generation scenarios. Therefore, in a frequently changing and unpredictable power system, either the full AC power flow or LODF-based method is recommended.

In the next section, the computational improvement of the contingency control method using the CNN method in contingency analysis is discussed.

Comparison of contingency control with or without CNN-based contingency analysis

As discussed in Section 3-4, the execution time of contingency control can potentially be reduced by 27% by using a more efficient contingency analysis algorithm, under the assumption that the number of required optimal power flow (OPF) executions is not influenced. This number could be influenced however, when the CNN-based contingency analysis method is significantly inaccurate, which could influence the number of identified insecure contingencies and thereby the number of OPF executions. The computational results of the DE-based method using the CNN approach for contingency analysis is shown in Table 4-5. It can be observed from this table that the required computational time for the contingency analysis operation is reduced compared to the method of Chapter 3. The total computational time of the new control method ranges between 238 and 1084 seconds, with an average of 580 seconds. This means that the average computational time is reduced by 40%. This reduction is larger than expected, since an maximum reduction of 27% was expected. However, this indicates that the CNN does not identify all insecure contingencies, due to which less OPF operations are performed. This is also shown in the results, since the average number of OPF operations is reduced from 2360 to 1970.

	OPF	Contingency analysis	Other operations
Average number of executions (-)	1970	800	-
Average computational time per execution (s)	0.31	0.065	-
Percentage of computation time	88%	8%	4%

Table 4-5: Computational effort of different contingency control process operations using CNN as contingency analysis

Further analysis of the contingency control results using a CNN as contingency analysis method shows that this method is considerably less conservative than the DE method of Chapter 3. It is found that in 82% of all results, the preventive control output of both methods was equal. This is the case when both methods results in full active power output for a particular controllable generator. In 10% of the cases, the method using CNN resulted in a higher power output than the original method. In 1% of all cases, this difference was more than 10%, with maximum of 35%. Since we assume the DE-based method of Chapter 3 to convergence to satisfactory accurate values, this indicates that the CNN-based approach does not identify certain critical contingencies. This leads to a higher control output, which could lead to potentially dangerous power grid scenarios.

4-3 Use of neural networks in contingency control

Instead of using a neural network only for the contingency analysis, this technique could also be applied to the complete contingency control algorithm. This novel strategy, or any machine

learning technique, has not been researched in previous academic literature for preventive-corrective control. However, machine learning is used before for corrective control strategies in [5,11,22,58]. Furthermore, the input information of contingency control is still in a grid-like topology and sparsely connected, which means that a data point is more closely related to its nearby data points than to more distant data points. Therefore, the convolutional neural network might still be preferable compared to a traditional neural network. However, this is not shown in previous researches and a comparison between the use of a convolutional neural network and a standard deep neural network will therefore be made.

In preventive-corrective control, the output of the neural network would preferable be the preventive and the corrective control actions. However, the number contingencies for which corrective control actions should be determined is not known a priori and also not constant. This is a complicating factor, since the number and shape of outputs of a neural network is generally known and constant. One could choose to set the corrective control actions equal to the preventive control actions, if there are no extra corrective control actions necessary. However, this would increase the output data dimension of the CNN hugely, since corrective control actions are defined for every contingency, without adding significant extra information.

4-3-1 Defining only preventive control actions using neural networks

The most important aspect of preventive-corrective control is to define preventive control actions within a short time frame. After all, computing the corrective control actions only takes the time of one OPF computation, if the preventive control actions are known. A potential solution to the output data dimension challenge could therefore be to only define the preventive control actions using the neural network. The preventive control action data set can be computed using the DE-based contingency control method discussed in this thesis. This way, the preventive control actions take into account the complicating coupling between the preventive and corrective control actions.

Furthermore, before computing the preventive control actions using the neural network, it should be checked whether any preventive measures are necessary. By doing this, there is no need to train the neural network for cases where no preventive control action is necessary. This should simplify the learning process of the network and reduce the amount of data required to acquire satisfactory accuracy. Defining whether any preventive control actions is required is does not require substantial computational effort: a single contingency analysis to define whether any contingency would cause grid limits to be violated and a subsequent optimal power flow for these identified contingencies will suffice to define whether preventive control actions are required to solve the optimisation problem.

4-3-2 Design of the neural networks

As an input for the neural network, the active and reactive power outputs of all grid buses are available. In this input data, the controllable generators are considered to deliver their maximum capacity. However, the reactive power is generally closely related to the active power for most buses, due to the constant power factor. Therefore, it is expected that only the active power values of the buses is sufficient to learn to accurately determine the preventive control actions. This reduces the amount of input data, without significantly reducing the

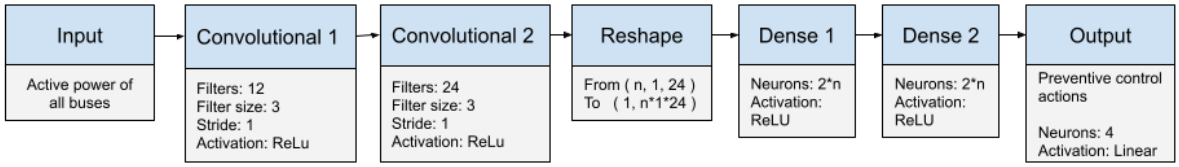

Figure 4-3: Convolutional neural network design for contingency control.

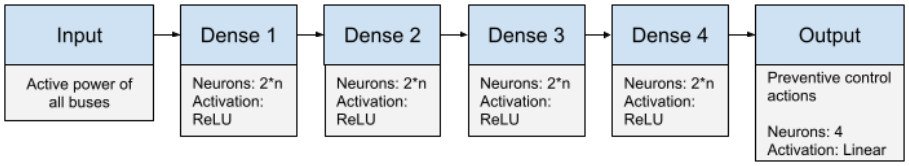

Figure 4-4: Neural network design without convolutional layers for contingency control

amount of information fed to the system, which increases the convergence time of the neural network. The output of the neural networks is a set of preventive control actions for the controllable DER.

As before-mentioned, the convolutional neural network is still expected to deliver superior results compared to a neural network without convolutional layers. However, since this has not yet been verified in academic literature, both types of networks are designed and evaluated. The designs of the neural networks with and without convolutional layers are shown in Fig. 4-3 and Fig. 4-4, respectively. In these figures, n is the number of buses. Compared to the CNN used for contingency analysis, the same number of convolutional filters and layers is used. For both layers, the number of neurons per dense layer is increased until no improvement in results was observed.

4-3-3 Data generation

The data for the contingency control neural network is generated using the DE-based method of Chapter 3. It is important that the data in this set is as accurate as possible, because the accuracy of the neural network heavily depends on the accuracy of the training data. Therefore, the data is generated using the control method with the full AC power flow analysis method, instead of the CNN-based analysis method. To generate the data, the Stedin Middelharnis power grid with load and generation data as discussed in Section 2-2 is used. The controllable DER connections are all set to maximum power output. The active power output of all buses is used as input for the neural network. The output of the neural network is the optimal preventive control action as defined by the optimisation problem in Chapter 3.

A total of 1972 of datapoints were acquired using the DE-based contingency control method. This data is again split into training (80%), validation (10%) and test data (10%).

4-3-4 Results

The results of the neural networks on cases where preventive control actions are required are presented in Table 4-6. Error ε is the error percentage between the preventive control

variable actions as determined by the DE-based contingency control method of Chapter 3 and the preventive control action output of the neural network. It can be observed that the convolutional neural network has superior performance in terms of output error compared to the neural network without convolutional layers. This confirms the hypothesis that the bus power input of the power grid is sparsely connected and therefore convolutional layers will be beneficial in predicting accurate preventive control measures.

Furthermore, the results of Table 4-6 show that the performance of the neural networks does not increase after 500 epochs. Given the small dataset of 1972, the networks might be prone to overfitting on this dataset after this large number of epochs. The evaluation time of the neural network is seconds, which is to times faster than the computation time of the DE-based control method. On average, it is times faster. This neural network approach is therefore extremely beneficial compared to the DE-based control method in terms of computational times. At the same time, after 500 epochs of neural network training, the mean error of the CNN is below 1% and the maximum output error for a single DER generator is 3.86%. This means that the CNN-based method is able to perform within reasonable accuracy, while displaying a vast increase in computational efficiency.

	No convolutional layers				Convolutional layers			
Epochs	Mean ε (%)	Max. ε (%)	Learning time (s)	Eval. time (s)	Mean ε (%)	Max. ε (%)	Learning time (s)	Eval. time (s)
100	1.62	8.83	472	0.044	1.07	6.19	592	0.045
200	1.34	12.68	903		1.16	4.97	1050	
500	0.97	4.24	2102		0.81	3.86	2489	
1000	0.96	5.42	4020		0.84	4.58	4822	

Table 4-6: Neural network results on contingency control with or without convolutional layers.

4-4 Conclusions

In this chapter, the application of (convolutional) neural networks on preventive-corrective control problem has been discussed. When the convolutional neural network is used to perform contingency analysis, the computational performance of the DE-based contingency control method is increased by 40%. However, the accuracy of the preventive control actions is affected, since not all critical contingencies are identified. Therefore, although this method increases the computational efficiency of the control, it is not recommended to use in practice. Also, this adjusted DE-based method is still computationally complex and not able to meet the computational performance requirements. Therefore, the approach where the coupled preventive control actions are determined by a neural network is also implemented and discussed. The computation time of the preventive control actions is decreased tremendously using this method, while the accuracy error is on average only 0.81% with a maximum of 3.86%. However, it should be noted that this neural network is prone to changes in the potential contingencies to be considered, any physical changes in the power grid, new controllable generators, or changes in any other constraints, such as the maximum curtailment ramp of the controllable generators. If any changes occur in these aspects, a new data set will have to be generated and the neural network should be retrained.

Chapter 5

Conclusions and recommendations

In a power grid system where corrective control actions are not sufficient for adequate contingency control and where preventive and corrective control actions are coupled, preventive-corrective contingency control is to be deployed. The contingency control method based on differential evolution (DE) as described and discussed in Chapter 3 is capable to determine suitable preventive and corrective control actions which satisfy the power grid and coupling constraints and minimize the power curtailment of the controllable distributed energy resources (DER) connections. Using preventive-corrective control, a significant amount of extra DER can be connected to the power grid without risking security limit violations in case of contingencies. Depending on the location of the DER generator in the grid of this study case, the amount of renewable energy which can be delivered to the distribution grid is increased by a factor 1.2 to 11.6, while less than 5% preventive power curtailment is required. However, this method is not capable to perform this preventive-corrective contingency control within reasonable time frame. The average computational time of the DE iteration for the Middelharnis power grid considered in this study is 970 seconds. In a dynamic distribution power grid, the grid situation can change significantly within this period of time, causing the control actions to be outdated and therefore inadequate. For larger power systems, the computational complexity would even increase further.

Machine learning techniques can be used to increase the computational efficiency of the contingency control process. A convolutional neural network (CNN) is capable to perform contingency analysis for different distribution power grids. Using a CNN-based method increases the computational efficiency of the contingency analysis by up to 17 times compared to the accurate full AC power flow method for the power grids in this case study. This factor is expected to increase when larger power grids are considered. The accuracy is only decreased by 0 to 5%, which is superior to the line outage distribution factor (LODF)-based contingency analysis method. However, it is found that using the CNN-based contingency analysis method in the contingency control strategy, the resulting preventive control actions can differ significantly from the optimal actions. This points toward the fact that not only contingencies which are just slight insecure are neglected, but also more severe contingencies. This means that the CNN-based contingency analysis method is not fit for this contingency control method.

The alternative of performing the complete preventive control determination using a neural network is also investigated. It is found that the convolutional neural network shows superior performance compared to the neural network without convolutional layers. This method delivers satisfactory accuracy results compared to the DE-based contingency control method, since an average deviation under 1% is found and a maximum deviation under 4%. Furthermore, this approach is computationally very efficient and able to compute preventive control actions in a fraction of a second.

For Stedin Netbeheer, the coupling between the preventive and corrective control actions is not as strict as in the case study of this thesis, since generators can be curtailed rather steep without the risk of grid instability. Therefore, it is advised to decouple the preventive and corrective control actions. In a preventive manner, controllable generators should be curtailed such that no grid component is overloaded and no voltage violations are present when no contingency has occurred. In case of a contingency, corrective control actions should be taken to mitigate the voltage or loading limit violations. These measures can be computed in a short time frame, since only one optimal power flow (OPF) operation is required.

5-1 Recommendations for future research

In further academic efforts, it is recommended to investigate several topics related to this research:

Improving OPF computations

It is advised to perform supplemental research on the computational complexity of the preventive-corrective control method based on DE, for example by performing the OPF operation using a method based on Machine learning (ML) or using an interior point algorithm.

Extend case study to large-scale transmission power grids

The benefit of the preventive-corrective control methods as discussed in this thesis might be most present in large-scale transmission power grids. In these grids, the restrictions on generator curtailment in case of emergency are more strict, since the transient stability of the grid might be affected by steep generator curtailment. Therefore, it is recommended to research the potential scenarios in transmission grids where preventive-corrective control might be required and test the methods of this thesis work on these scenarios.

Investigate business case for preventive-corrective control

It would be interesting to study the potential business case of preventive-corrective control, considering the amount of extra DER which could be connected to the grid and the compensation costs for the curtailment of these generators. These study cases should be performed for different-sized distribution and transmission power grids, considering the curtailment limits in practice and the saved grid expansion costs.

Extend dataset for contingency control neural network

Generation of the dataset for the contingency control neural network as described in Section 4-3 is computational complex, since it relies on the control method as described in Chapter 3. Therrefore, the dataset used in this thesis work was limited. The accuracy of this method could potentially be increased using an increased amount of data. In further research, the influence of using a larger data set could be investigated.

Appendix A

Additional contingency control results

In this appendix, additional results on different designs of the preventive-corrective contingency control method based on differential evolution can be found.

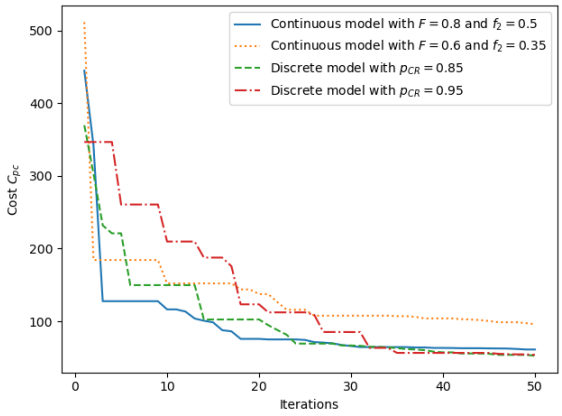

(a) Population size $2D$

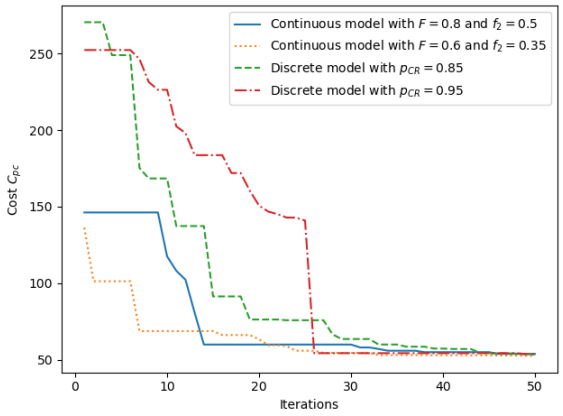

(b) Population size $5D$

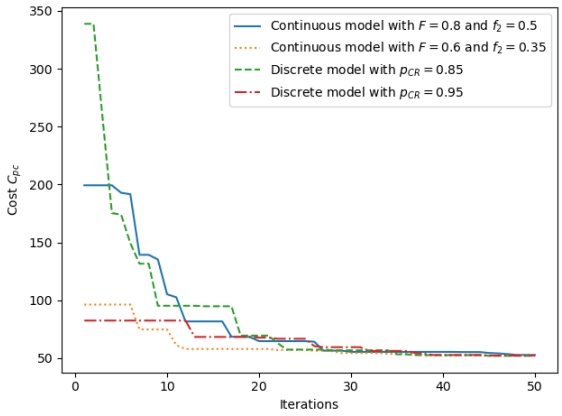

(c) Population size $10D$

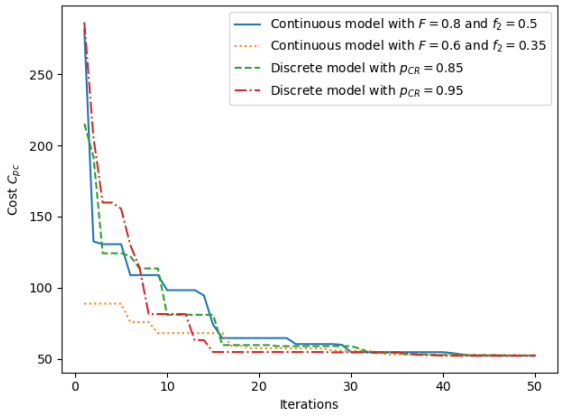

(d) Population size $20D$

Figure A-1: Preventive control cost evolution for different model designs on June 2nd, given different population sizes.

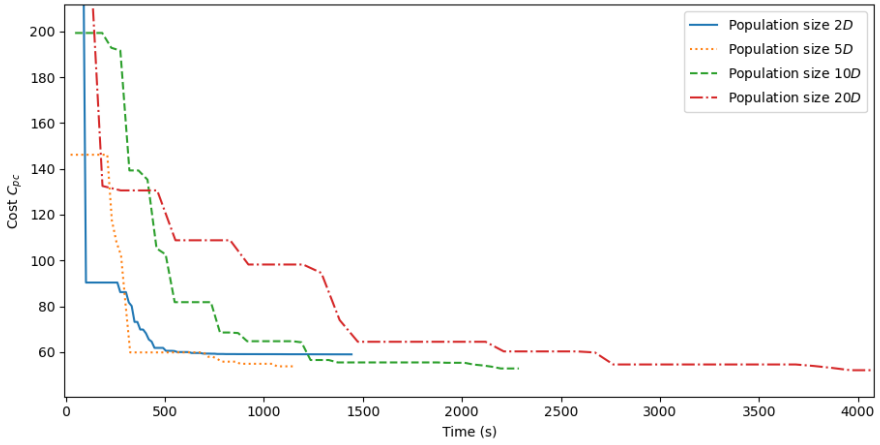

Figure A-2: Preventive control cost evolution for different population sizes on June 2nd.

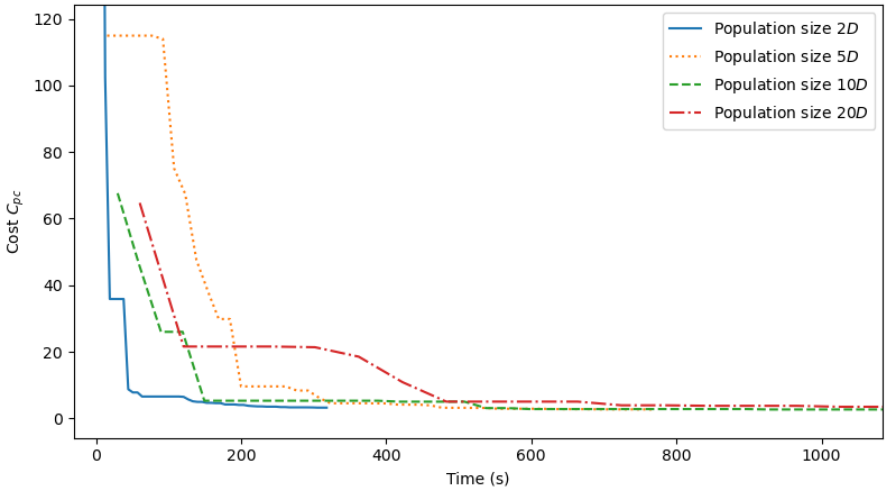

Figure A-3: Preventive control cost evolution for different population sizes on April 15$^{\text{th}}$.

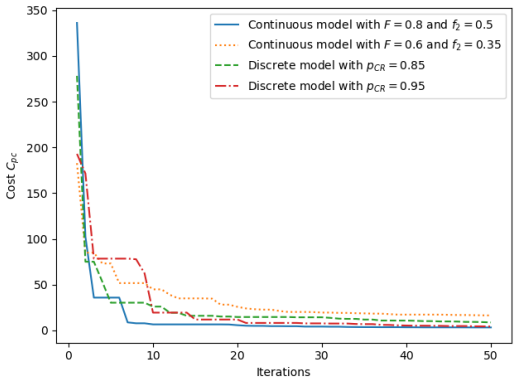

(a) Population size $2D$

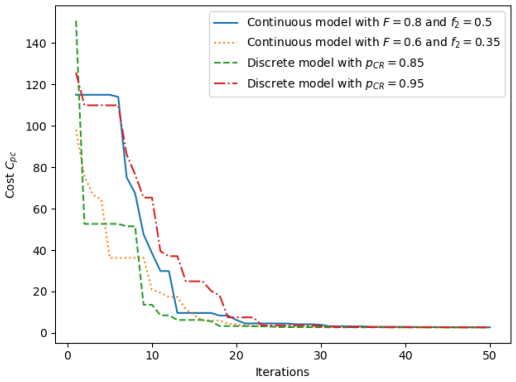

(b) Population size $5D$

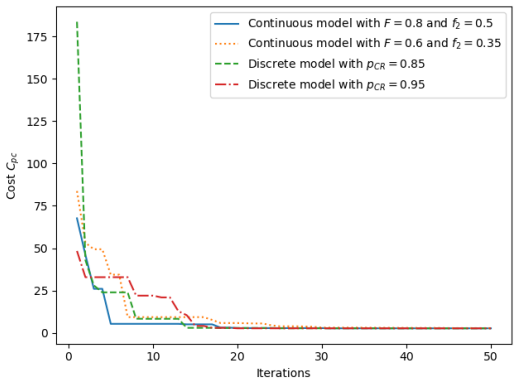

(c) Population size $10D$

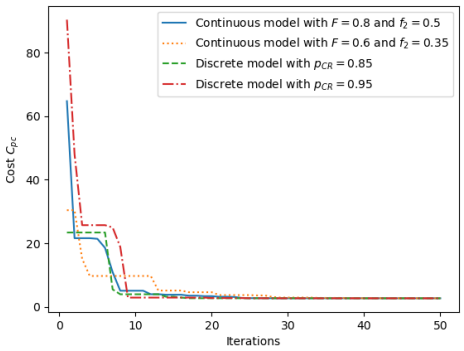

(d) Population size $20D$

Figure A-4: Preventive control cost evolution for different model designs on April 15$^{\text{th}}$, given different population sizes.

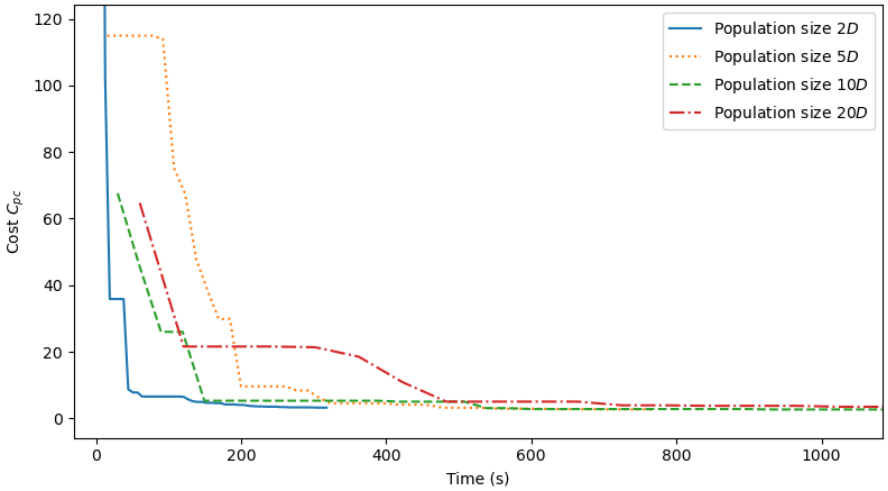

Figure A-5: Preventive control cost evolution for different population sizes on April 15$^{\text{th}}$.

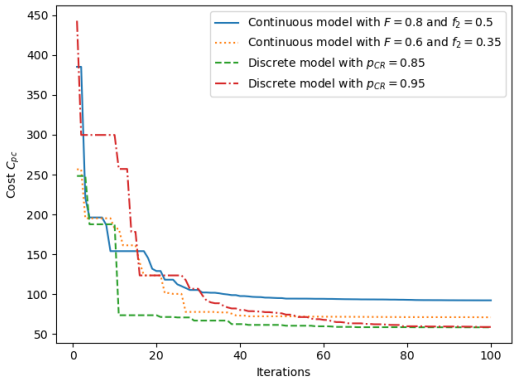

(a) Population size $2D$

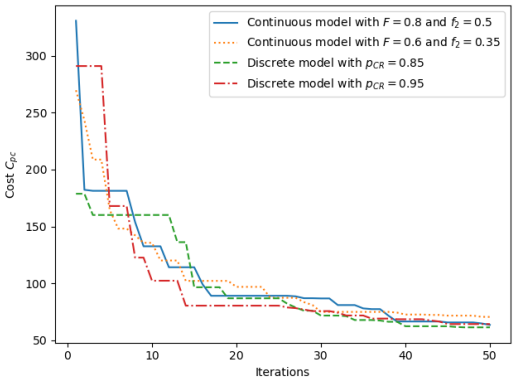

(b) Population size $5D$

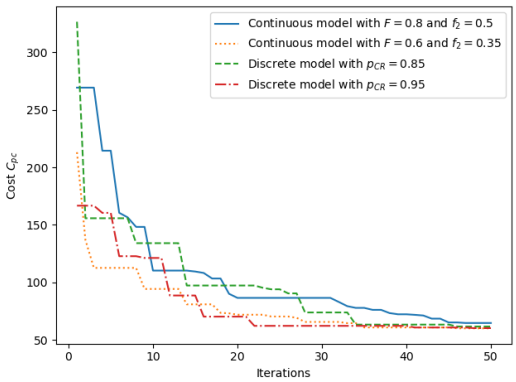

(c) Population size $10D$

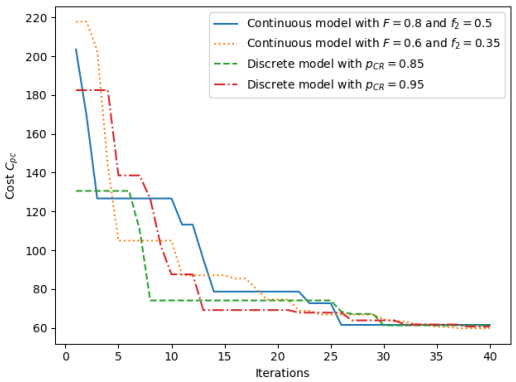

(d) Population size $20D$

Figure A-6: Preventive control cost evolution for different model designs on August 4$^{\text{th}}$, given different population sizes.

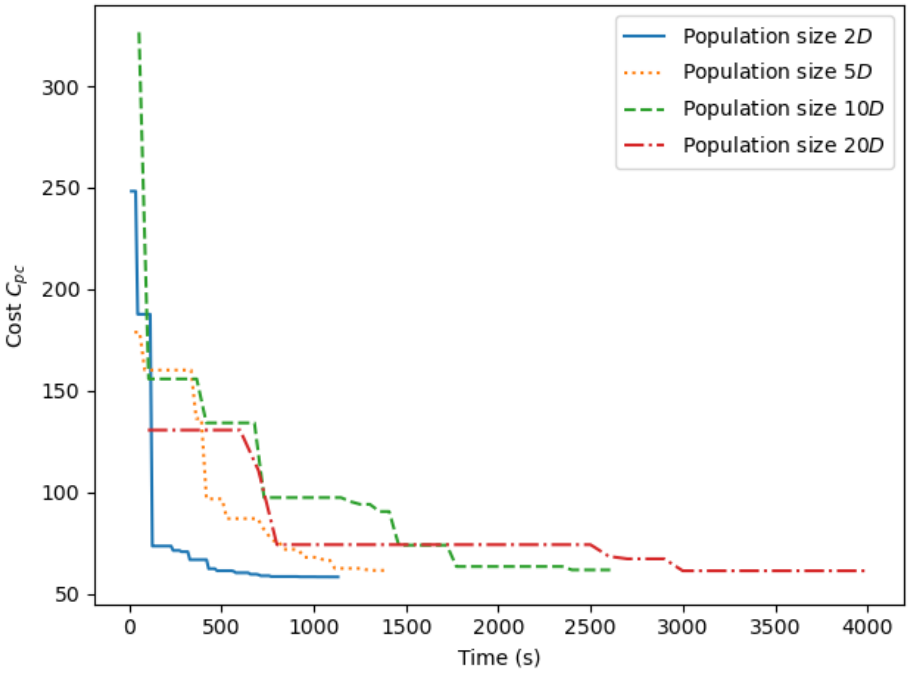

Figure A-7: Preventive control cost evolution for different population sizes on August 4$^{\text{th}}$.

Bibliography

[1] T. Athay, R. Podmore, and S. Virmani, "A Practical Method for the Direct Analysis of Transient Stability," *IEEE Transactions on Power Apparatus and Systems*, vol. PAS-98, no. 2, 3 1979.

[2] G. W. Ault, R. A. Currie, and J. R. McDonald, "Active power flow management solutions for maximising DG connection capacity," in *2006 IEEE Power Engineering Society General Meeting, PES*. IEEE Computer Society, 2006.

[3] Autoriteit Consument en Markt, "Netcode Elektriciteit," 5 2016. [Online]. Available: https://wetten.overheid.nl/BWBR0037940

[4] C. Baskin, N. Liss, E. Zheltonozhskii, A. M. Bronstein, and A. Mendelson, "Streaming Architecture for Large-Scale Quantized Neural Networks on an FPGA-Based Dataflow Platform," in *2018 IEEE International Parallel and Distributed Processing Symposium Workshops (IPDPSW)*. IEEE, 5 2018.

[5] F. Bellizio, S. Karagiannopoulos, P. Aristidou, and G. Hug, "Optimized Local Control for Active Distribution Grids using Machine Learning Techniques," in *IEEE Power and Energy Society General Meeting*, vol. 2018-August. IEEE Computer Society, 12 2018.

[6] G. Ben-Yaacov, G. Mijne, and K. Struwig, "Fast Decoupled Load Flow for Security Assessment," *IFAC Proceedings Volumes*, vol. 13, no. 8, 1980.

[7] A. S. Bouhouras, C. Iraklis, G. Evmiridis, and D. S. Labridis, "Mitigating Distribution Network congestion due to high DG penetration," in *IET Conference Publications*, vol. 2014, no. CP665. Institution of Engineering and Technology, 2014.

[8] F. Capitanescu, T. V. Cutsem, and L. Wehenkel, "Coupling optimization and dynamic simulation for preventive-corrective control of voltage instability," *IEEE Transactions on Power Systems*, vol. 24, no. 2, pp. 796–805, 2009.

[9] Conseil international des grands reseaux electriques. Comite d'etudes C6., *Benchmark systems for network integration of renewable and distributed energy resources*. Paris: CIGRÉ, 2014, vol. 1.

[10] Delft University of Technology, "The Dutch PV Portal," 2021. [Online]. Available: https://www.tudelft.nl/en/ewi/over-de-faculteit/afdelingen/electrical-sustainable-energy/photovoltaic-materials-and-devices/dutch-pv-portal

[11] R. Dobbe, O. Sondermeijer, D. Fridovich-Keil, D. Arnold, D. Callaway, and C. Tomlin, "Toward Distributed Energy Services: Decentralizing Optimal Power Flow with Machine Learning," *IEEE Transactions on Smart Grid*, vol. 11, no. 2, pp. 1296–1306, 3 2020.

[12] M. J. Dolan, E. M. Davidson, I. Kockar, G. W. Ault, and S. D. McArthur, "Distribution power flow management utilizing an online optimal power flow technique," *IEEE Transactions on Power Systems*, vol. 27, no. 2, pp. 790–799, 5 2012.

[13] Y. Du, F. Li, J. Li, and T. Zheng, "Achieving 100x Acceleration for N-1 Contingency Screening with Uncertain Scenarios Using Deep Convolutional Neural Network," *IEEE Transactions on Power Systems*, vol. 34, no. 4, pp. 3303–3305, 7 2019.

[14] G. Ejebe and B. Wollenberg, "Automatic Contingency Selection," *IEEE Transactions on Power Apparatus and Systems*, vol. PAS-98, no. 1, 1 1979.

[15] Enexis Netbeheer, "Wetswijziging: Reservecapaciteit gebruiken voor energie-opwek," 1 2021. [Online]. Available: https://www.enexis.nl/over-ons/nieuws/2021/01/wetswijziging-reservecapaciteit-gebruiken-voor-energie-opwek

[16] Fang Da-Zhong, Song Wen-Nan, and T. S. Chung, "A modification to the fast decoupled load flow for power system with low X/R ratio branches," in *1993 2nd International Conference on Advances in Power System Control, Operation and Management, APSCOM-93.*, 12 1993, pp. 279–284.

[17] J. M. Gimenez Alvarez, "Critical Contingencies Ranking for Dynamic Security Assessment Using Neural Networks," in *2009 15th International Conference on Intelligent System Applications to Power Systems*. IEEE, 11 2009.

[18] Government of The Netherlands, "Climate Policy." [Online]. Available: https://www.government.nl/topics/climate-change/climate-policy

[19] J. Hazra and A. K. Sinha, "A risk based contingency analysis method incorporating load and generation characteristics," *International Journal of Electrical Power and Energy Systems*, vol. 32, no. 5, pp. 433–442, 6 2010.

[20] S. Huang, Q. Wu, Z. Liu, and A. H. Nielsen, "Review of congestion management methods for distribution networks with high penetration of distributed energy resources," in *IEEE PES Innovative Smart Grid Technologies Conference Europe*, vol. 2015-January, no. January. IEEE Computer Society, 1 2015.

[21] IPCC, "Climate Change 2021: The Physical Science Basis. Contribution of Working Group I to the Sixth Assessment Report of the Intergovernmental Panel on Climate Change ," Cambridge University Press, Tech. Rep., 2021.

[22] S. Karagiannopoulos, P. Aristidou, and G. Hug, "Data-Driven Local Control Design for Active Distribution Grids Using Off-Line Optimal Power Flow and Machine Learning Techniques," *IEEE Transactions on Smart Grid*, vol. 10, no. 6, pp. 6461–6471, 11 2019.

[23] D. P. Kingma and J. Ba, "Adam: A Method for Stochastic Optimization," 12 2014.

[24] R. E. Larson, W. F. Tinney, and J. Peschon, "State Estimation in Power Systems Part I: Theory and Feasibility," *IEEE Transactions on Power Apparatus and Systems*, vol. PAS-89, no. 3, pp. 345–352, 3 1970.

[25] Laura Rodríguez, "Solar panel orientation: How using East-West structures improves the performance of your project," 6 2021. [Online]. Available: https://ratedpower.com/blog/solar-panel-orientation/

[26] Y. LeCun, B. Boser, J. S. Denker, D. Henderson, R. E. Howard, W. Hubbard, and L. D. Jackel, "Backpropagation Applied to Handwritten Zip Code Recognition," *Neural Computation*, vol. 1, no. 4, 12 1989.

[27] A. Monticelli, A. Garcia, and O. Saavedra, "Fast decoupled load flow: hypothesis, derivations, and testing," *IEEE Transactions on Power Systems*, vol. 5, no. 4, pp. 1425–1431, 1990.

[28] NEDU, "Verbruiksprofielen," 2021. [Online]. Available: https://www.nedu.nl/documenten/verbruiksprofielen/

[29] Netbeheer Nederland, "Netbeheerders publiceren actuele schaarstegebieden," 10 2019. [Online]. Available: https://www.netbeheernederland.nl/nieuws/netbeheerders-publiceren-actuele-schaarstegebieden-1308

[30] ——, "Capaciteitskaart invoeding elektriciteitsnet," 12 2021. [Online]. Available: https://capaciteitskaart.netbeheernederland.nl/

[31] T. Ochi, D. Yamashita, K. Koyanagi, and R. Yokoyama, "The development and the application of fast decoupled load flow method for distribution systems with high R/X ratios lines," in *2013 IEEE PES Innovative Smart Grid Technologies Conference (ISGT)*. IEEE, 2 2013.

[32] Paul M. Anderson and A. A. Fouad, "The Elementary Mathematical Model," in *Power System Control and Stability*, 2nd ed. Wiley-IEEE Press, 2013, ch. 2, pp. 13–52.

[33] D. Rajicic and A. Bose, "A modification to the fast decoupled power flow for networks with high R/X ratios," *IEEE Transactions on Power Systems*, vol. 3, no. 2, 5 1988.

[34] K. Rudion, A. Orths, Z. A. Styczynski, and K. Strunz, "Design of benchmark of medium voltage distribution network for investigation of DG integration," in *2006 IEEE Power Engineering Society General Meeting, PES*. IEEE Computer Society, 2006.

[35] F. Schafer, J.-H. Menke, and M. Braun, "Contingency Analysis of Power Systems with Artificial Neural Networks," in *2018 IEEE International Conference on Communications, Control, and Computing Technologies for Smart Grids (SmartGridComm)*. IEEE, 10 2018.

[36] V. Schepel, A. Tozzi, M. Klement, H. Ziar, O. Isabella, and M. Zeman, "The Dutch PV portal 2.0: An online photovoltaic performance modeling environment for the Netherlands," *Renewable Energy*, vol. 154, 7 2020.

[37] A. R. Seifi, M. R. Hesamzadeh, N. Hosseinzadeh, and A. R. Malekpour, "An optimal load shedding approach for distribution networks with DGs considering capacity deficiency modelling of bulked power supply," Tech. Rep., 2009. [Online]. Available: https://www.researchgate.net/publication/224400850

[38] P. Sekhar and S. Mohanty, "Power system contingency ranking using Newton Raphson load flow method," in *2013 Annual IEEE India Conference (INDICON)*. IEEE, 12 2013.

[39] Stedin Netbeheer, "Capaciteit van het elektriciteitsnet," 10 2021. [Online]. Available: https://www.stedin.net/zakelijk/congestiemanagement-en-transportprognoses/beschikbare-netcapaciteit

[40] ——, "'Groeipijn' op het elektriciteitsnet van Goeree-Overflakkee," 4 2021. [Online]. Available: https://www.stedin.net/over-stedin/pers-en-media/persberichten/groeipijn-op-het-elektriciteitsnet-van-goeree-overflakkee

[41] R. Storn and K. Price, "Differential Evolution – A Simple and Efficient Heuristic for global Optimization over Continuous Spaces," *Journal of Global Optimization*, vol. 11, no. 4, pp. 341–359, 1997.

[42] B. Stott, "Review of load-flow calculation methods," *Proceedings of the IEEE*, vol. 62, no. 7, 1974.

[43] B. Stott and O. Alsac, "Fast Decoupled Load Flow," *IEEE Transactions on Power Apparatus and Systems*, vol. PAS-93, no. 3, 5 1974.

[44] R. Sunitha, R. S. Kumar, and A. T. Mathew, "Online static security assessment module using artificial neural networks," *IEEE Transactions on Power Systems*, vol. 28, no. 4, pp. 4328–4335, 2013.

[45] UNFCCC Authors, "The Paris Agreement," 2015. [Online]. Available: https://unfccc.int/process-and-meetings/the-paris-agreement/the-paris-agreement

[46] ——, "Glasgow Climate Pact," 11 2021. [Online]. Available: https://unfccc.int/documents/310475

[47] R. van Amerongen, "A general-purpose version of the fast decoupled load flow," *IEEE Transactions on Power Systems*, vol. 4, no. 2, pp. 760–770, 5 1989.

[48] R. Vykuka and L. Nohacova, "Fast-decoupled method for contingency analysis," in *Proceedings of the 2014 15th International Scientific Conference on Electric Power Engineering (EPE)*. IEEE, 5 2014.

[49] ——, "Sensitivity factors for contingency analysis," in *2015 16th International Scientific Conference on Electric Power Engineering (EPE)*. IEEE, 5 2015.

[50] K. P. Wong and Z. Dong, "Differential Evolution, an Alternative Approach to Evolutionary Algorithm," in *Modern Heuristic Optimization Techniques*. Hoboken, NJ, USA: John Wiley & Sons, Inc., 2008, ch. 9, pp. 171–187.

[51] A. J. Wood, B. F. Wollenberg, and G. B. Sheblé, *Power Generation, Operation, and Control*, 3rd ed. Hoboken, New Jersey: Wiley, 12 2013.

[52] L. Wu, J. Gao, G. Kumar Venayagamoorthy, and R. G. Harley, "On Artificial Intelligence Approaches for Contingency Analysis in Power System Security Assessment 1, 2," Tech. Rep., 2018.

[53] L. Wu, G. K. Venayagamoorthy, R. G. Harley, and J. Gao, "Cellular Computational Networks based Voltage Contingency Ranking Regarding Power System Security," in *2018 Clemson University Power Systems Conference (PSC)*. IEEE, 9 2018.

[54] Y. Xu, Z. Y. Dong, R. Zhang, K. P. Wong, and M. Lai, "Solving preventive-corrective SCOPF by a hybrid computational strategy," *IEEE Transactions on Power Systems*, vol. 29, no. 3, pp. 1345–1355, 2014.

[55] Y. Xu, H. Yang, R. Zhang, Z. Y. Dong, M. Lai, and K. P. Wong, "A contingency partitioning approach for preventive-corrective security-constrained optimal power flow computation," *Electric Power Systems Research*, vol. 132, pp. 132–140, 3 2016.

[56] S. Yang, B. Vaagensmith, and D. Patra, "Power Grid Contingency Analysis with Machine Learning: A Brief Survey and Prospects," in *2020 Resilience Week (RWS)*. IEEE, 10 2020.

[57] H. Yuan and Y. Xu, "Preventive-Corrective Coordinated Transient Stability Dispatch of Power Systems with Uncertain Wind Power," *IEEE Transactions on Power Systems*, vol. 35, no. 5, pp. 3616–3626, 9 2020.

[58] S. Zarrabian, R. Belkacemi, and A. A. Babalola, "Reinforcement learning approach for congestion management and cascading failure prevention with experimental application," *Electric Power Systems Research*, vol. 141, pp. 179–190, 12 2016.

[59] Q. Zhou and J. W. Bialek, "Generation curtailment to manage voltage constraints in distribution networks," *IET Generation, Transmission and Distribution*, vol. 1, no. 3, pp. 492–498, 2007.

[60] J. Zhu, "Optimal Power Flow," in *Optimization of Power System Operation*. Hoboken, NJ, USA: John Wiley & Sons, Inc, 1 2015.

[61] ——, "Power Flow Analysis," in *Optimization of Power System Operation*. Hoboken, NJ, USA: John Wiley & Sons, Inc, 1 2015.

Glossary

List of Acronyms

DER	distributed energy resources
OPF	optimal power flow
CNN	convolutional neural network
FDLF	fast decoupled load flow
ML	Machine learning
LODF	line outage distribution factor
PTDF	power transfer distribution factor
DE	differential evolution